SEARS FOUNDATION FOR MARINE RESEARCH
BINGHAM OCEANOGRAPHIC LABORATORY, YALE UNIVERSITY

JOURNAL OF
MARINE RESEARCH

VOLUME 13 1954 NUMBER 2

WIND MIXING CURRENTS[1]

By

JOHN C. FREEMAN, JR.

Agricultural and Mechanical College of Texas
College Station, Texas

ABSTRACT

A wind system may create an ocean current by differential mixing in a two layer ocean; such a current may be imposed on other currents due to the wind. In one situation studied, such differential mixing produced an average transport of water about 10 to 20 % of the transport due to wind stress.

WIND ACTION ON THE OCEAN

Sverdrup, et al. (1942: 489–503) have summarized the processes through which wind causes currents in the ocean:

a) currents directly driven by wind stress;

b) mass transport of water by wind waves;

c) currents caused by redistribution of density by wind transport.[2]

In addition, wind also causes mixing between the cold thermocline waters and the warm surface layer of the ocean. The following discussion shows that, through such mixing action, the wind may cause an additional current (in an ocean with a stable density stratification).

[1] Contribution No. 35, Department of Oceanography, Agricultural and Mechanical College of Texas.

[2] Reference to this process was suggested by R. S. Arthur.

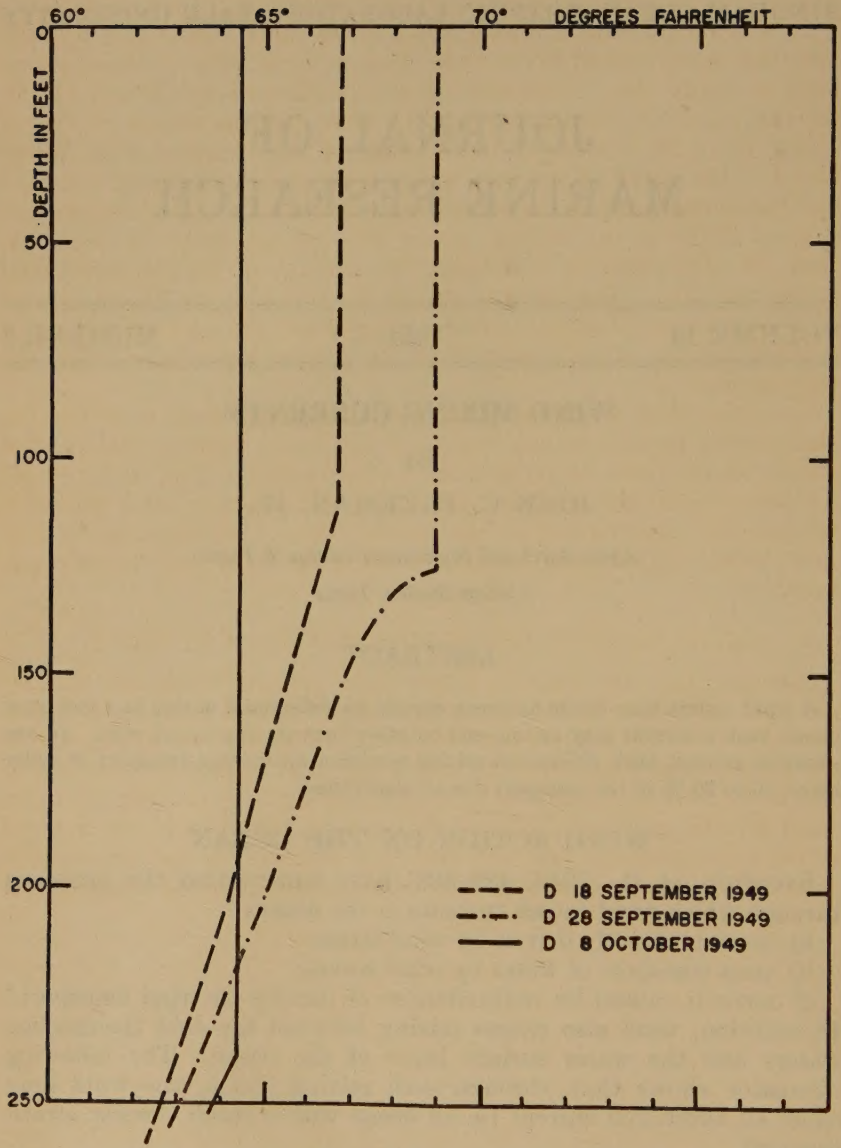

Figure 1. The warming at 44°N 41°W during the period 18 September to 28 September 1949 occurred when the winds were Beaufort Force 4. Between 28 September and 8 October the column cooled by a large amount and the winds were Beaufort Force 5½.

It is assumed that a strong wind mixes more cold water upward into the warm mixed layer than does a weak wind. Observations tend to verify this. Consider the ship station at 44° N and 41° W for the period 18 September to 8 October 1949 as shown in Fig. 1. From 18 to 28 September the average of the Beaufort wind forces was 4. The depth of the then-mixed layer remained almost constant and the temperature of the surface layer increased. These occurrences suggest little or no mixing across the thermocline. In contrast, from 28 September to 8 October the average of the Beaufort wind forces was 5½. During this period the mixed layer cooled almost 5° F and deepened about 110 feet, suggesting the upward mixing of a large amount of cold water into the surface layer from below the thermocline.

Consider that a strong wind with associated mixing across the thermocline persists in one section of the ocean while a weaker wind which causes little or no mixing occurs nearby. The colder water introduced into the surface layer under the stronger wind will alter the density distribution in the surface layer. In response to this new density distribution, a current will occur within the upper ocean layers.

EVALUATING THE WIND MIXING CURRENT

Assume that the ocean is a two-layer system which has initially constant densities in the upper and lower layers and no currents. Strong winds over a portion of the ocean will then cause mixing across the thermocline (boundary) so that a region of relatively colder water will be formed in the surface layer of the ocean. Neglecting the other wind effects, such a horizontal variation in the density distribution of the ocean surface layer will lead to a current. It will be assumed that, after transient effects have disappeared, such a current will be in geostrophic balance so that

$$u = -\frac{1}{\rho' f}\frac{\partial p}{\partial y} \tag{1}$$

$$v = \frac{1}{\rho' f}\frac{\partial p}{\partial x}, \tag{2}$$

where u and v are the ocean velocity components in the x- and y-directions respectively, ρ' the ocean density at a given point (x,y) in the surface layer, f the Coriolis parameter (vertical component of the earth's vorticity), and p the pressure.

The hydrostatic equation is

$$p(z) = p_0 + g\rho' z, \tag{3}$$

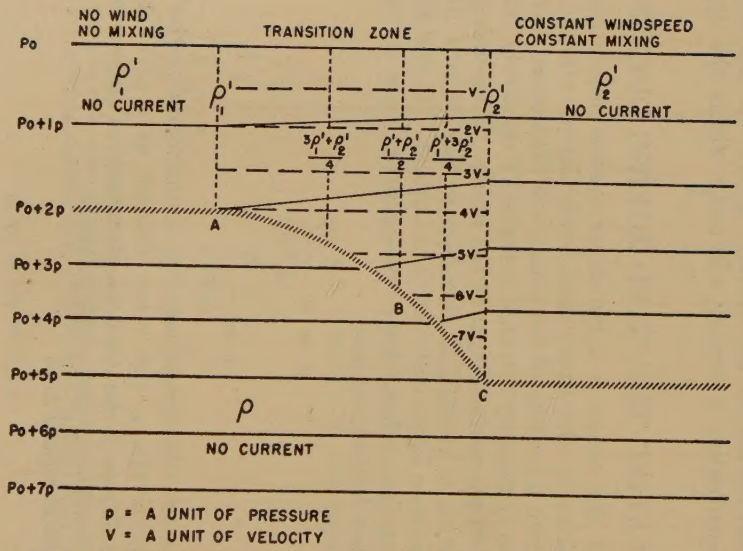

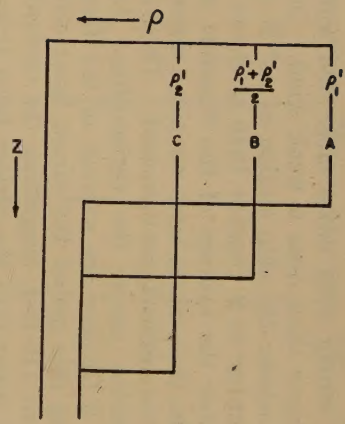

Figure 2. Variations in the mixing cause horizontal variations in the density which lead to a current that increases with depth. The current at the bottom of the mixed layer must balance the slope of the thermocline if there is no current in the lower layer.

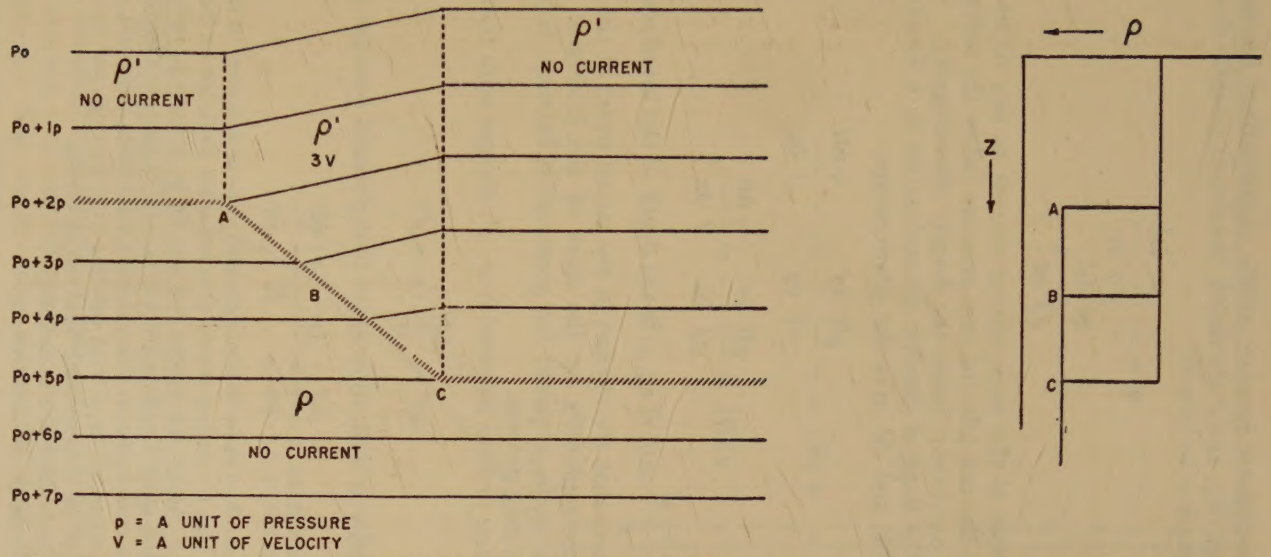

Figure 3. An adaptation of an illustration in Sverdrup "*The Oceans*" showing a current constant in the horizontal and with depth in a layer of constant density. (Between A and C)

where p_0 is atmospheric pressure at the ocean surface (assumed constant here), g gravity, and z[3] the depth (measured positive downward). We use this equation to obtain:

$$u = -\frac{gz}{\rho' g}\frac{\partial \rho'}{\partial y} \tag{4}$$

$$v = \frac{gz}{\rho' f}\frac{\partial \rho'}{\partial x}. \tag{5}$$

This is a measure of the wind mixing current at any depth z. The mixing process has not affected any pressure below the surface layer. Hence there is no current below the density discontinuity. Margules formulae[4] for the slope of density discontinuities on a rotating earth, together with (4) and (5), give the relationships

$$u\,(H) = -\frac{gH}{\rho' f}\frac{\partial \rho'}{\partial y} = -\frac{\gamma}{f}\frac{\partial H}{\partial y} \tag{6}$$

and

$$v\,(H) = \frac{gH}{\rho' f}\frac{\partial \rho'}{\partial x} = \frac{\gamma}{f}\frac{\partial H}{\partial x}, \tag{7}$$

where $\gamma = g\dfrac{\rho - \rho'}{\rho'}$ and $H\,(x, y)$ is the depth of the interface. These expressions assert that the current in the mixed water at the interface is balanced geostrophically by the slope of the interface. We can show that this slope, required for geostrophic balance, is a natural result of the mixing process.

For the mixing process assumed here, ρ' changes such that

$$\Delta\rho' = \frac{\Delta H}{H}(\rho - \rho'). \tag{8}$$[5]

Equation (8) tells us that, since space changes exist because of mixing,

$$\frac{\partial \rho'}{\partial x} = \frac{(\rho - \rho')}{H}\frac{\partial H}{\partial x}. \tag{9}$$

[3] By using the depth of water from a horizontal plane as a measure of the pressure, we are assuming that the mixing process does not affect the height of the horizontal surface. Dr. R. S. Arthur has pointed out that 100 m of water at salinity 35 °/₀₀, with the upper 50 m at 20° C and the lower 50 m at 10° C, mixes to a length 100 m less 1 cm, so that the mixing process does not leave the surface horizontal. Mr. R. O. Reid has kindly computed the current resulting from the slope and has found that it is 10% or less of the corresponding wind mixing current.

[4] See any standard reference in meteorology.

[5] Δ is any small change or the differential.

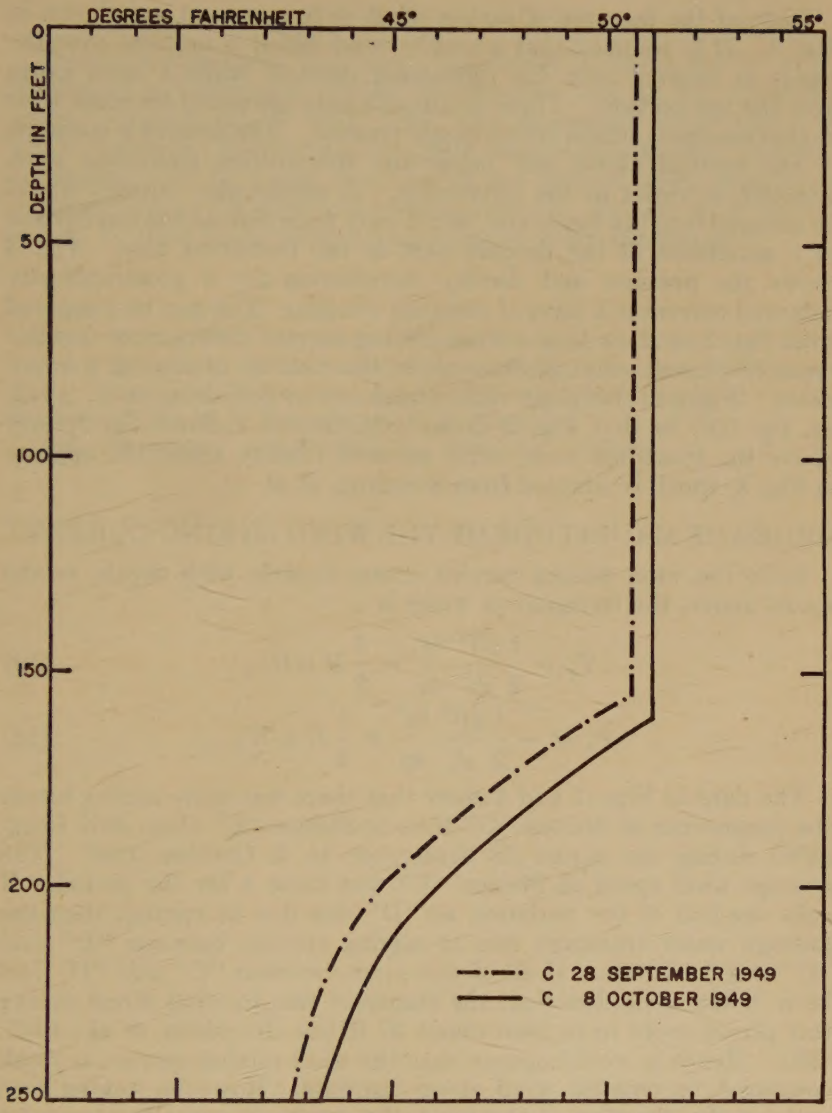

Figure 4. The small amount of mixing at Lat. 53N, Long. 35W is illustrated here. This is to be compared with the large amount of mixing at Station "D" for the same period (Fig. 1).

This is essentially the same as equation (7), which is an independent relation between two expressions for the velocity. Thus the slope of the interface that results from mixing balances the geostrophic current created by mixing.

Some of the features of such a wind mixing current are shown in Fig. 2. It is assumed that a steady wind which is uniform over the region is blowing over the right-hand portion, while a calm exists over the left portion. These conditions have prevailed for some time so that transient effects are no longer present. The density is constant in the vertical above and below the thermocline transition zone, although it varies in the x-direction. A geostrophic current would be directed into the figure and would vary from zero at the top surface to a maximum at the deepest part of the transition zone. Fig. 3 shows the pressure and density distribution for a geostrophically balanced current in a layer of constant density. This can be compared with Fig. 2 to show how a wind mixing current differs from familiar types of currents that must occur in the vicinity of sloping thermoclines. Fig. 2 of this paper differs from one by Sverdrup, et al. (1942: 44, fig. 106) in that Fig. 2 shows a horizontal variation in density above the transition zone, while no such density transition appears in Fig. 3, which is adapted from Sverdrup, et al.

ORDER OF MAGNITUDE OF THE WIND MIXING CURRENT

Since the wind mixing current varies linearly with depth, in the model above, the transport of water is

$$T_y = \frac{1}{2}\frac{gH^2}{\rho' f}\frac{\partial \rho'}{\partial x} = \frac{1}{2} H\, v(H)\,, \tag{10}$$

$$T_x = -\frac{1}{2}\frac{gH^2}{\rho' f}\frac{\partial \rho'}{\partial y} = \frac{1}{2} H\, u(H)\,. \tag{11}$$

The data in Figs. 1 and 4 show that there was more mixing across the thermocline at Station "D" than at Station "C" (Lat. 53N Long. 35W) during the period 28 September to 8 October 1949. The average wind speed at Station "C" was force 4 for the period. If only one-half of the variation at "D" was due to mixing, then the average water transport due to mixing current between "D" and "C" was 0.4 ft²/sec. If all of the winds between "C" and "D" had been in the same direction, the transport due to wind stress during this period could have been about 27 ft²/sec (Sverdrup, et al., 1942: 498). Hence it would appear that the wind mixing current is small compared to possible wind stress currents. However, taking into account the direction of the wind, the resultant stress transport for this period was 2 to 5 ft²/sec.[6] Thus the wind mixing current was 10 to 20% of the net transport by the wind stress for this 10-day period.

[6] This is probably a maximum estimate, since each wind is assumed to give the maximum possible transport.

ACKNOWLEDGMENTS

This work, stimulated by contact with Henry Stommel and W. V. R. Malkus at a Conference on the Thermocline held at Big Meadows Lodge, Virginia, 25–27 May 1953, was performed under Office of Naval Research Contract N7 onr 48703, Project NR 083-061. Messrs. C. Sparger and G. Jung, members of the project, made significant contributions to the style and technical detail. Messrs. R. S. Arthur and R. O. Reid made helpful contributions to the discussion.

Leipper, D. F. and R. M. Adams
1952. Summary of North Atlantic Weather Station data. Tech. Rep. No. 3, Agricultural and Mechanical College of Texas, Texas A and M Research Foundation Project 29, ONR Contract N7 48703, NR 083–061. 2 pp.
Sverdrup, H. U., M. W. Johnson and R. H. Fleming
1942. The oceans. Prentice-Hall, Inc., New York. 1060 pp.

DEPOSITION OF SALTS FROM SEA WATER BY FRIGID CONCENTRATION[1]

By

KURT H. NELSON AND THOMAS G. THOMPSON

Department of Oceanography
University of Washington
Seattle, Washington

ABSTRACT

The order of formation of solid phases when sea water freezes has been investigated down to −40° C. About 80% of the water present in the original quantity of sea water is transformed into ice before the first salt crystallizes. Sodium sulfate decahydrate, the first salt formed, begins to separate at −8.2° C and the sulfate concentration in the brine decreases markedly. When the freezing point reaches −22.9° C, sodium chloride dihydrate precipitates in large quantities. The concentration of sodium in the brine decreases rapidly as the freezing point decreases below −22.9° C. There is a decrease in the concentrations of magnesium and potassium in the brine below −36.0° C when potassium chloride and magnesium chloride dodecahydrate precipitate. Thermal analyses indicate that calcium chloride hexahydrate begins to form at −54° C. The last of the brine probably solidifies at a temperature slightly below −54° C.

INTRODUCTION

One of the earlier studies on the sequence of salt deposition by the evaporation of sea water was made by Usiglio (1849). Since then, the chemical processes and changes that occur during the evaporation of sea water have been rather thoroughly investigated. van't Hoff, together with a number of co-workers (1905, 1909), studied the equilibria between various salts at 25° and 83° C in order to explain the origin of the strata of the famous Stassfurt salt deposits. D'Ans (1933) and others established the equilibrium conditions in detail for the chlorides and sulfates of sodium, potassium, calcium and magnesium at temperatures from 0° to 120° C. A summary of present knowledge concerning the deposition of oceanic salts during the evaporation of sea water is given by Phillips (1947).

On the other hand, only meager information appears to be available concerning the deposition of salts when sea water is concentrated by freezing. Since prehistoric times, inhabitants of the polar regions

[1] The authors wish to acknowledge financial aid from the Office of Naval Research under provisions of Contract N8onr–520/III between the Office of Naval Research and the University of Washington.

have obtained sodium chloride by this method. The removal of the ice as it formed on ponds of sea water resulted in a concentrated brine from which sodium chloride would precipitate on further freezing. More generally, however, the concentrated brine was evaporated over fires in order to secure the salt.

In experiments on the freezing of sea water, Ringer (1906) found that ice was the only solid formed during the interval from the initial freezing point to about −8.2° C. The precipitation of the first salt, sodium sulfate, occurred from about −8.2° to approximately −23° C, and this was followed by the deposition of the dihydrate of sodium chloride at temperatures below −23° C. Ringer supposed that magnesium chloride precipitation began at −36° C. The disappearance of a portion of the potassium from the brine between −36° and −40° C was presumably due to formation of either potassium chloride or a double salt with magnesium chloride. The end point at which all of the liquid had become solid was postulated as being slightly below the eutectic point of calcium chloride. However, few data are available in support of this order of precipitation.

Thus the object of the present study was to investigate the actual deposition of the various salts by the frigid concentration of sea water.

METHODS AND APPARATUS

Source of Sea Water. Surface sea water was collected in seasoned 25 and 50 liter glass carboys about 100 miles off the Washington Coast at 47° 52.5′ N and 126° 17.0′ W. The sea water was filtered through a sintered glass filter of F porosity. The chlorinity of the sea water was 18.01 ‰.

Apparatus. Temperatures were measured by means of calibrated Western Electric 14B Thermistors and a Wheatstone bridge. To permit immersion of the thermistors in the brines, they were sealed in glass tubes that contained a drop of mercury for thermal conduction.

The apparatus used in freezing the sea water samples consisted of (1) a freezer capable of maintaining any temperature down to −45° C with a variation of ±3° C, (2) a three liter freezing container with a removable bottom, (3) a freezing tube with a capacity of about 500 ml, and (4) two concentration vessels of 8 and 50 liter capacities for concentrating the sea water by freezing.

The freezer was 197 cm long, 78 cm wide and 89 cm high, with an interior opening 100 cm long, 33 cm wide and 27 cm deep. Extending downward from the bottom of this interior opening were three wells 23 cm in diameter and 25 cm deep. The cooling coils, positioned behind the sheet metal interior walls, did not extend down around the

wells. The insulation in the walls, bottom and lid consisted of cork slabs 15 cm thick, and the exterior finish was Masonite. The refrigerator unit was a Frigidaire Meter Miser MM-3 compressor unit that employed F12 as the coolant.

The three liter freezing container, shown in Fig. 1, consisted of a Lucite cylinder 13 cm in diameter by 30.5 cm high clamped to a removable Lucite bottom. The lower end of the cylinder was machined to give a close fit with the bottom. Lucite blocks 2.5 by 3.8 by 1.3 cm were cemented on the exterior near the bottom to aid in clamping the cylinder and bottom together.

The bottom was constructed from a Lucite disk 14 cm in diameter and 1.3 cm thick. A shallow cone was machined in the upper surface of the disk leaving a ridge to position a rubber gasket between the cylinder and the bottom. In the center of the bottom was a tapped drainage hole that extended through a small Lucite block cemented to the underside of the disk. This hole was closed by a plastic screw plug fitted with a rubber gasket and a brass rod handle. The clamping device consisted of a plywood disk and ring held together by long bolts.

An air inlet tube was placed in the container by means of a rubber stopper and wire framework. This tube consisted of a length of 8 mm Pyrex tubing sealed at the lower end and flanged at the top. After the container had been filled with sea water, the top was covered with heavy gauge aluminum foil fastened in place with tape to prevent the loss of water by evaporation.

The freezing tube, constructed from a vertical Lucite tube 45 cm long and 3.8 cm in diameter, was closed at the bottom with a removable stopper, which was a close-fitting one hole rubber stopper inserted in the tube and expanded to give a tight fit. The expansion was accomplished by tightening a wing nut on a machine screw that passed through the hole in the stopper. Washers on each side of the stopper held the machine screw in place and aided in the expansion of the stopper. The washer and head of the machine screw were coated with neoprene paint to prevent corrosion and subsequent contamination of the brines. During the freezing of the brine, an air inlet tube was positioned in the freezing tube, and the top was closed with heavy gauge aluminum foil.

Since only a small amount of brine remained at the lower temperatures, large quantities of sea water were subjected to a preliminary concentration by freezing, and the resulting brines were then used for the low temperature investigations. Two concentration vessels were constructed for this purpose.

The small concentration vessel, pictured in Fig. 2, was converted from a bell jar of nine liters capacity. A one hole rubber stopper and

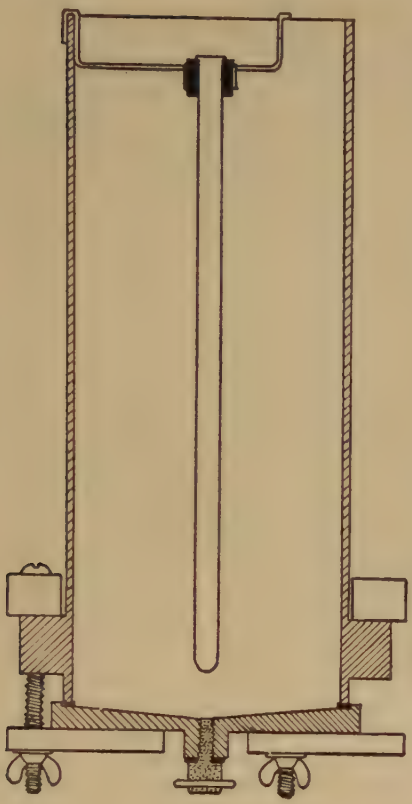

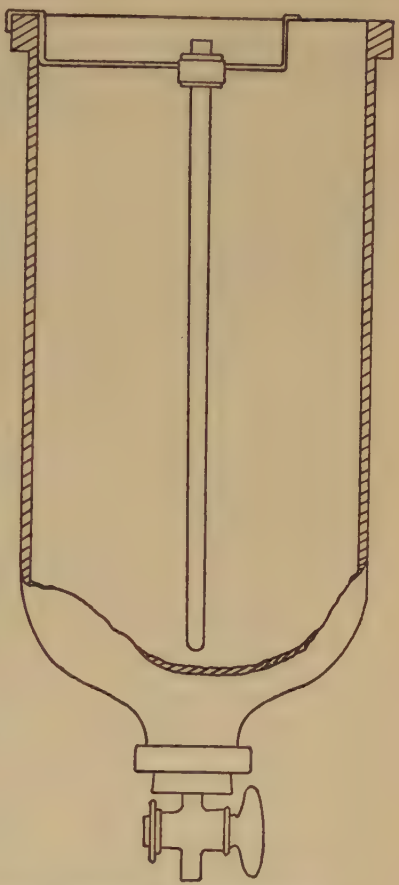

Figure 1 (left). Lucite container with capacity of 3 liters for freezing samples.
Figure 2 (right). Container of 9 liters capacity for concentrating brine by freezing.

a stopcock were used to close the small opening in the neck of the bell jar. After the bell jar had been inverted, the wire framework holding the air inlet tube was placed in position. The top of the vessel was covered with heavy gauge aluminum foil after the vessel had been filled with sea water.

The large concentration vessel, shown in Fig. 3, was 72.5 cm long, 24.0 cm wide and 55.5 cm high. The sloping bottom was 41.5 cm below the top edge along the sides of the vessel and 47.5 cm below the top at the center of the bottom. The tank was fabricated from Lucite sheets 6 mm thick; a 2.5 by 3.8 by 22.5 cm Lucite block was cemented

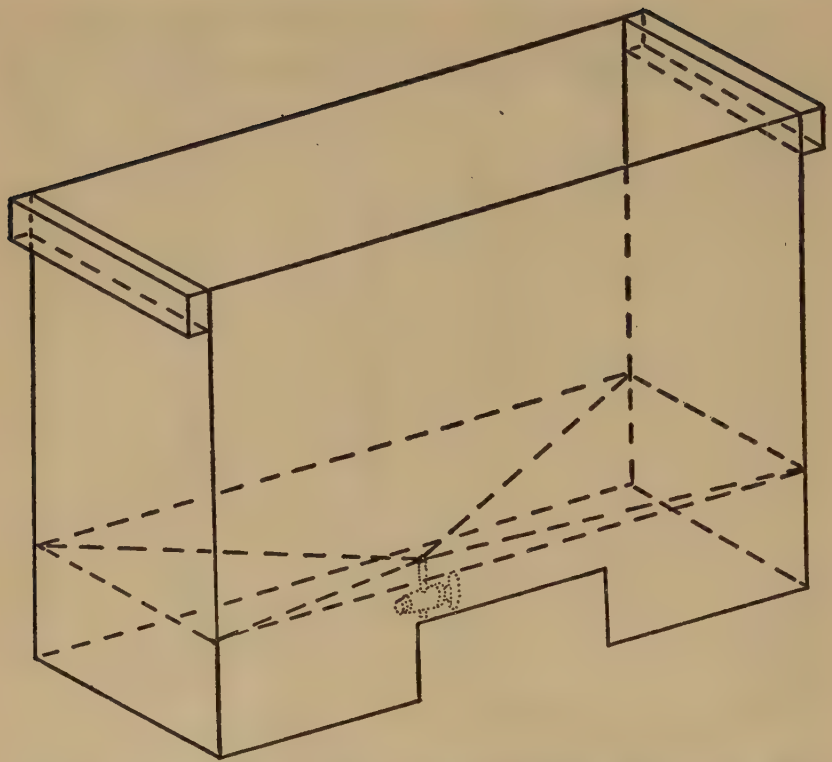

Figure 3. 100 liter lucite container for concentrating large volumes of sea water by freezing.

along the top edge of each end for a handle. Drainage of the brine was through a stopcock fastened to a short plastic tube cemented to the center of the bottom. An air inlet tube was positioned in the vessel by a wire framework. Heavy gauge aluminum foil fastened with tape closed the top of the vessel during the freezing of the sea water.

Freezing of Samples. To obtain brines and salts, the temperature of a sample of sea water was lowered to a desired value, after which the brine, salts and ice were separated. The freezing procedure varied somewhat depending upon the desired final temperature of the brine.

The entire freezing process for each of the first 18 samples in Table I was conducted in the freezing container. After being filled with three liters of filtered sea water, the container was placed in a well in the freezer. The container sides were insulated with tightly packed cloth in order to enhance freezing downward from the top. After the freez-

TABLE I. Quantity of Brine Remaining from One Kilogram of Sea Water and Concentrations of the Major Ions in Brines with Various Freezing Points

Sample No.	*Freezing Point (°C)*	*Brine (g)*	*Na (‰)*	*Mg (‰)*	*Ca (‰)*	*K (‰)*	*Cl (‰)*	*SO_4 (‰)*
1	− 2.20	696.2	12.05	1.65	0.48	0.44	22.80	—
2	− 4.40	309.4	23.23	3.19	0.86	0.85	42.71	5.97
3	− 5.50	212.3	28.39	3.92	1.02	1.03	51.18	—
4	− 6.10	205.9	30.44	4.34	1.11	1.12	56.49	—
5	− 6.90	147.1	33.42	4.83	1.21	1.24	62.41	8.61
6	− 8.30	89.9	37.87	5.66	1.38	1.42	71.89	—
7	− 8.60	68.7	38.76	5.81	1.42	1.46	74.47	8.85
8	− 9.60	79.3	41.19	6.31	1.54	1.58	81.01	—
9	−10.60	66.1	43.69	6.79	1.65	1.68	87.31	5.48
10	−10.75	49.3	44.18	6.83	1.66	1.70	87.98	—
11	−13.10	39.3	49.44	7.74	1.89	1.94	99.73	3.81
12	−14.70	27.8	53.13	8.29	2.03	2.10	107.08	—
13	−15.20	34.3	54.12	8.50	2.08	2.15	109.82	—
14	−16.25	25.5	56.36	8.86	2.17	2.25	114.30	2.69
15	−18.50	27.2	61.23	9.67	2.36	2.46	123.27	—
16	−19.20	21.3	62.67	9.86	2.42	2.54	126.61	—
17	−20.60	25.2	65.81	10.31	2.48	2.67	131.72	1.77
18	−22.20	15.0	68.83	10.86	2.59	2.79	138.91	—
19	−23.25	35.9	69.35	11.65	2.84	3.11	142.37	—
20	−23.75	34.5	65.86	13.62	3.18	3.53	144.02	—
21	−24.70	14.4	60.02	16.63	3.98	4.48	146.11	—
22	−25.60	9.9	54.17	19.77	4.76	5.10	147.78	—
23	−26.40	7.9	48.57	22.41	5.57	6.01	149.12	1.06
24	−27.90	2.8	40.03	27.19	6.66	7.41	152.33	—
25	−29.95	3.6	30.15	34.35	8.09	9.24	155.96	0.69
26	−32.90	2.6	20.53	43.20	9.68	12.21	161.01	—
27	−34.90	1.8	16.08	48.58	10.77	15.05	165.83	—
28	−36.25	1.0	14.22	50.77	12.02	19.29	166.78	—
29	−36.55	0.9	13.76	50.36	14.52	20.31	167.49	—
30	−40.20	0.5	10.90	46.89	44.74	16.75	173.49	—
31	−43.15	0.3	8.49	58.96	10.53	13.84	174.60	—

ing point had reached the desired value, the sealed end of the air inlet tube was broken off with a long rod in order to insert the thermistor into the brine for temperature measurements. After the brine was drained off through the drainage hole in the bottom, the bottom of the container was removed and the salts were transferred to a small specimen jar. Although most of the salt crystals were found on the bottom of the container, there were a few crystals adhering to the under surface of the ice. It was found that this occurred more frequently as the temperature decreased. The ice was allowed to melt after

another bottom was fastened to the cylinder. After the quantities of brine and water from the melted ice were determined, samples of the brine were taken for analysis.

The sea water used for each of Samples 19 through 22 was subjected to a preliminary concentration by freezing. Eight liters of sea water were allowed to freeze to a temperature of about −8° C in the small concentration vessel. After the brine was transferred to the freezing container, the freezing was continued in the manner described for the first samples.

For Samples 23 through 25, 50 liters of sea water were frozen in the large concentration vessel until the freezing point of the brine was around −8° C. The resulting brine was divided into three equal portions. Each portion was then frozen individually in the freezing container in a manner analogous to that of the first samples.

For each of the remaining samples, 50 liters of sea water were first concentrated by freezing to −17° C in the large concentration vessel, after which they were concentrated further by freezing to −25° C in the small concentration vessel. The brine was then transferred to the freezing tube, and the freezing was continued in a manner similar to the procedure used for the first samples.

Identification of Salts. The salts were identified by microscopical chemical reactions of the ions which constitute the salts and by the optical properties of the salts as determined with a petrographic microscope. The ions present in a salt were identified by qualitative analysis carried out on a microscope slide under a petrographic microscope (Chamot and Mason, 1948).

Analysis of Brines. For some analyses, a 25 ml sample of the brine was diluted to one liter in a Normax volumetric flask. Aliquots were taken from this solution for analysis.

Sodium and Potassium Ions. The concentrations of sodium and potassium ions in the brines were determined by means of a Beckman Model DU Spectrophotometer with the Flame Photometry Attachment Model 9200. The 2,000 megohm resistor was replaced with a 10,000 megohm resistor to increase the sensitivity of the instrument five times. A series of standard solutions with compositions covering the range of concentrations in the diluted brines were prepared from distilled water and Baker's Analyzed Grades of sodium chloride, potassium chloride, magnesium carbonate, and calcium carbonate. The carbonates were dissolved in a minimum amount of C.P. hydrochloric acid. For determining sodium, the percent transmission was obtained first for the low standard, then for the diluted brine, then for the high standard, and finally for the flame background with distilled

water. This procedure was repeated twice and the readings for each solution were averaged. The flame background was subtracted from the transmission readings of the standards and of the diluted brine before graphical interpolation was applied to find the concentration of sodium in the diluted brine. The sodium concentration in the undiluted brine was then calculated. A similar procedure was followed in determining the concentrations of potassium in the brines.

Calcium Ion. A 25 ml aliquot of the diluted brine was treated with a buffer solution of 1 N sodium hydroxide to raise the pH to about 10 so as to precipitate the magnesium. Three drops of a saturated aqueous solution of ammonium purpureate were added as the indicator. The ammonium purpureate solution should be freshly prepared each day due to decomposition of the indicator when it is in solution form. The aliquot was then titrated with a 0.01 N standard disodium (ethylenedinitrilo)-tetraacetate solution until its color matched that of a comparison solution which consisted of two drops of cresol red indicator solution in 50 ml of a saturated borax solution.

Magnesium Ion. To a 25 ml aliquot of the diluted brine, 1 ml of buffer solution was added to raise the pH to about 10 without precipitating the magnesium. The buffer solution was composed of 67.5 g of ammonium chloride dissolved in 570 ml of concentrated ammonium hydroxide, and enough water was added to make one liter. Five drops of indicator solution, consisting of 0.50 g Eriochromeschwarz-T dissolved in 100 ml of ethanol, were added to the aliquot. The sum of calcium and magnesium ions in the aliquot was titrated with a 0.01 N standard disodium (ethylenedinitrilo)-tetraacetate solution until the color of the aliquot matched that of a comparison solution consisting of one drop of bromophenol blue indicator solution in 50 ml of saturated borax solution. The concentration of magnesium ion was obtained by the calcium titration above.

Chloride Ion. The concentration of chloride ion in a brine was determined by a Mohr chloride titration. 25 ml aliquots of the diluted brines were titrated with 0.1 N standard silver nitrate solution by using 1 ml of a saturated potassium chromate solution as the indicator.

Sulfate Ion. Gravimetric sulfate determinations were made on the brines by the procedure described by Thompson, et al. (1931). For the brines with freezing points above $-17°$ C, a weighed 25 ml sample was used. The size of the sample was increased for the brines with lower freezing points.

Thermal Analysis. Thermal analyses were made on sea water samples and several brines. For all samples except 29 and 31, 10 ml of the sea water or brine under examination were placed in a small

test tube containing a thermistor. A smaller volume of brine was used for Samples 29 and 31. The sample was frozen in an acetone-dry ice bath so that the frozen mass surrounded the thermistor. The frozen sample was removed from the bath and was placed in a cotton-filled can 22 cm high by 9 cm in diameter. The interior of the cotton packing had been cooled for several hours with dry ice in a test tube. The thermistor was connected to the Wheatstone bridge and the tem-

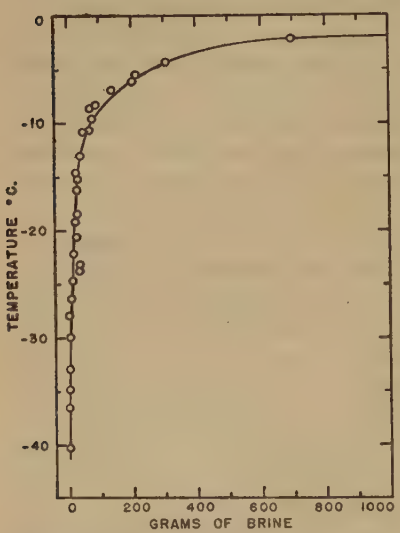

Figure 4. Grams of unfrozen brine remaining after freezing 1 kilogram of sea water at various temperatures.

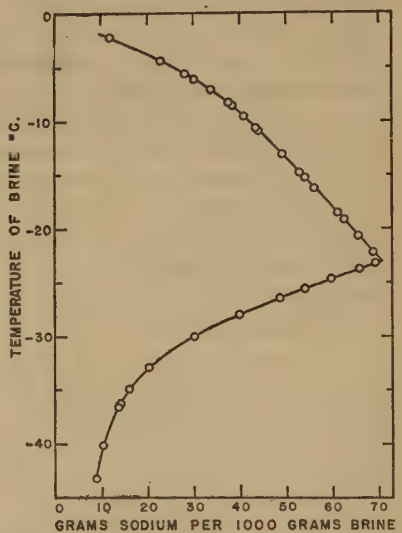

Figure 5. Concentration of sodium in brines in equilibrium with salts and ice at various temperatures.

perature was determined at intervals as the frozen sample slowly melted. Depending upon the rate of change of the temperature, the intervals varied from periods as short as 20 seconds to as long as two minutes or more. A time-temperature curve was then plotted for the sample.

RESULTS

Quantity of Brine. The amount of brine in equilibrium with the ice when one kilogram of sea water was frozen to various temperatures is shown in Fig. 4 from data in Table I. Note that a large portion of the water was transformed into ice during the initial stages of freezing. Approximately 80% of the water had solidified when the temperature had decreased to only −6° C. Below this temperature, the amount of ice formed was small.

Analysis of Brines. The results of the analyses for the major ions in each brine are given in Table I and in Figs. 5–10.

Concentration of Sodium. From the initial freezing point of sea water to −8.2° C, the concentration of sodium in the brine continually increased. In the range −8.2° to −22.9° C, the increase was slightly less due to the formation of sodium sulfate decahydrate. A marked decrease in the sodium concentration occurred in brines with freezing

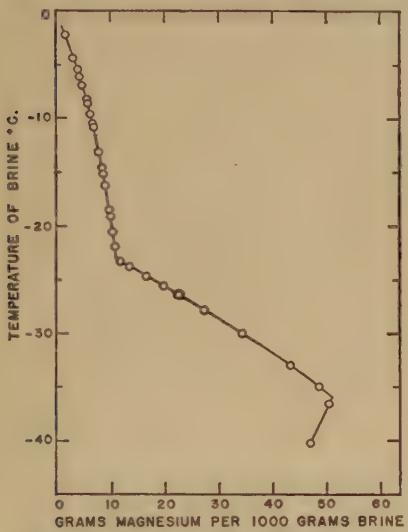

Figure 6. Concentration of magnesium in brines in equilibrium with salts and ice at various temperatures.

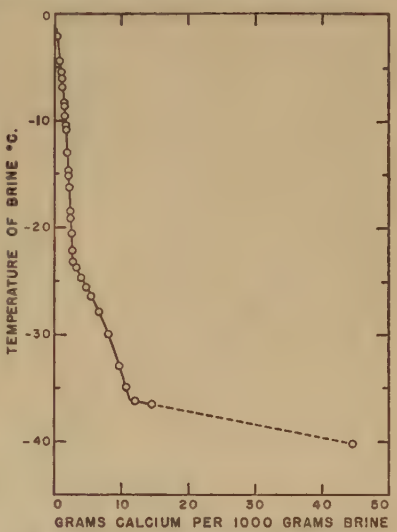

Figure 7. Concentration of calcium in brines in equilibrium with salts and ice at various temperatures.

points below −22.9° C due to precipitation of large quantities of sodium chloride dihydrate (see Fig. 5).

Concentration of Magnesium. Until the freezing point reached −22.9° C, the concentration of magnesium in the brine increased gradually as ice and sodium sulfate decahydrate crystallized from the brine. During the formation of sodium chloride dihydrate between −22.9 and −36.0° C, the increase in magnesium content of the brine decreased as the freezing point was lowered below −36.0° C. This was due to the crystallization of magnesium-containing salts (see Fig. 6).

Concentration of calcium. In Fig. 7 the concentration of calcium in the brine is shown as a function of the temperature. From the initial freezing point of sea water to −22.9° C there was a slow increase in the concentration of calcium in the brine as ice and sodium sulfate

decahydrate formed. Between −22.9 and −36.0° C the formation of a large amount of sodium chloride dihydrate removed a considerable amount of water from the brine. This resulted in a fourfold increase in the calcium concentration in the brine. Below −36.0° C, the concentration of calcium in the brine increased considerably.

When the temperatures of the separated brines rose, precipitation of calcium carbonate occurred. Generally, the time interval before

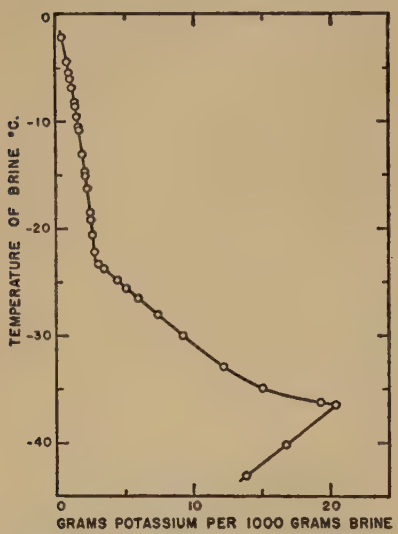

Figure 8. Concentration of potassium in brines in equilibrium with salts and ice at various temperatures.

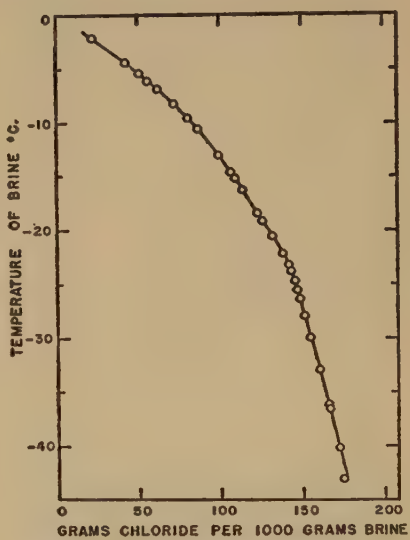

Figure 9. Concentration of chlorides in brines in equilibrium with salts and ice at various temperatures.

precipitation was perceptibly decreased as the temperature decreased and the salinity of the brine increased. Thus, for brines with temperatures somewhat below the freezing point of the sea water, a period of several days at room temperature was required before any precipitate was visible. This time interval had decreased to several hours when the temperatures of the brines were slightly above −22.9° C. The brines with freezing points between −22.9 and −36.0° C showed a precipitate from a few hours to less than an hour after separation of the brine. Precipitation occurred almost immediately after separation of the brine from the salts and ice when the temperatures of the brine were below −36.0° C. Storing the brines at temperatures somewhat above their freezing points lengthened the time before any precipitate was evident.

Concentration of Potassium. There was a gradual increase in concentration of potassium in brines until a temperature −22.9° C was reached. The removal of a large amount of water below −22.9° C as sodium chloride dihydrate resulted in a considerable increase in the potassium concentration in the brine. Below −36.0° C the decrease in the potassium content indicated the formation of potassium-containing salts (see Fig. 8).

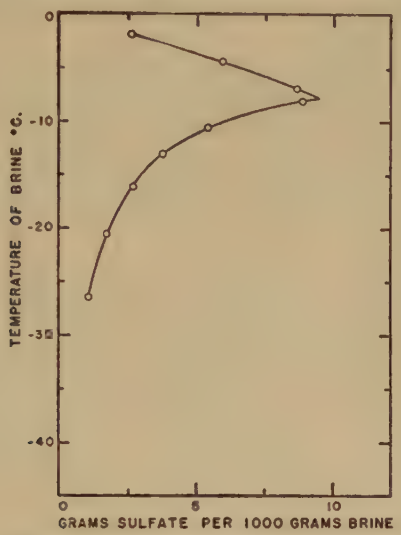

Figure 10. Concentration of sulfates in brines in equilibrium with salts and ice at various temperatures.

Concentration of Chloride. The concentrations of chloride in brines with various freezing points are illustrated in Fig. 9. The removal of water from the brine as ice and as water of crystallization in sodium sulfate decahydrate resulted in a continuous increase in the concentration of chloride until the temperature reached −22.9° C. Below this temperature, the chloride participated in the formation of salts, and therefore the increase in chloride concentration was less than that at higher temperatures.

For calculating the freezing point of sea water from its chlorinity, Thompson (1932) gave the equation

$$T = -0.0966\ Cl - 0.0000052\ \mathrm{Cl}^3,$$

where T is the freezing point in degrees Centigrade and Cl is the chlorinity. This equation fits the data in Table I until the chlorinity

has reached about 50 ‰, but it deviates increasingly at higher chlorinities. From the data in Table I, recomputation of the coefficients in Thompson's equation yielded the following:—

$$T = -0.0966\ Cl - 0.0000035\ Cl^3,$$

where T and Cl have the same meaning as before. This new equation is valid for chlorinities of about 50 to 140 ‰. At higher chlorinities, the chloride begins to precipitate as sodium chloride dihydrate and the equation becomes invalid.

Concentration of Sulfate. The change in the concentration of sulfate in the brine as the temperatures decreased is portrayed in Fig. 10. Until the temperature reached −8.2° C, the change in sulfate concentration was that due to the removal of water as ice from the brine. Beginning at −8.2° C, sodium sulfate decahydrate crystallized from the brine and thereby caused the concentration of sulfate in the brine to decrease rapidly.

Thermal Analysis. The time-temperature curves obtained for samples of sea water and several brines are shown in Fig. 11. For clarity, the curves have been displaced to the right from zero time. All the time-temperature curves had a small plateau at −38.87° C due to the melting of the mercury in the thermistor assembly.

The time-temperature curve for Puget Sound sea water showed a plateau above −5° C which resulted from the melting of the ice. The inflection point at −22.9° C in the curve arose from the dissolving of the sodium chloride dihydrate.

The sea water from 47° 52.5′ N and 126° 17.0′ W, with a chlorinity of 18.01 ‰, gave a time-temperature curve similar to the curve obtained with Puget Sound sea water of chlorinity 16.50 ‰. A very small inflection point occurred in the curve at −36.0° C.

Inflection points in the time-temperature curves for the brines of Samples 2, 9 and 17 were the same as those in the curves for sea water. However, due to the higher salt content of the brines, the curves had more distinct inflection points. As the chlorinity of the brine increased, the inflection points at −22.9 and −36.0° C enlarged into plateaus while the plateau for the melting of the ice decreased in size and occurred at a lower temperature. In the curve for Sample 17, the plateau resulting from the melting of the ice disappeared, which indicates that only a small amount of ice forms at the lower freezing temperatures.

The time-temperature curves for the brines of Samples 23 and 26 showed a broadening of the −36.0° C inflection point into a plateau. Simultaneously in the curve for Sample 23, the plateau due to the

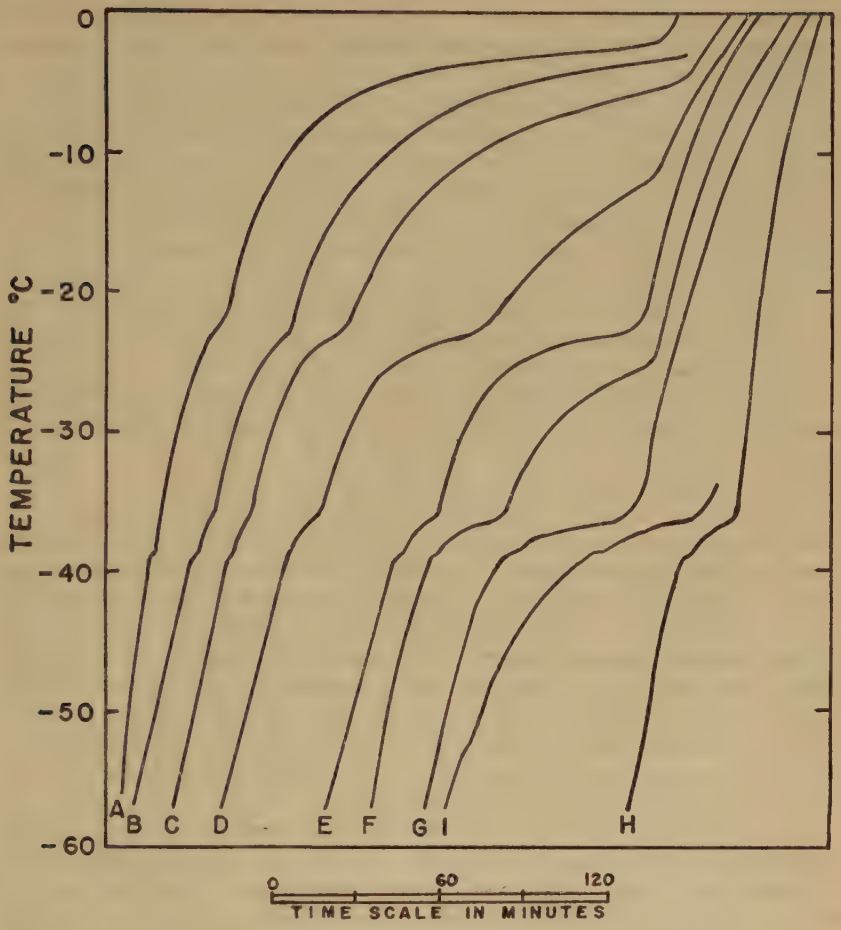

A	SEA WATER PUGET SOUND	CHLORINITY	16.50 ‰
B	SEA WATER 47° 52.5' N 126° 17.0' W	CHLORINITY	18.01 ‰
C	BRINE FROM SAMPLE 2	CHLORINITY	42.71 ‰
D	BRINE FROM SAMPLE 9	CHLORINITY	87.31 ‰
E	BRINE FROM SAMPLE 17	CHLORINITY	131.72 ‰
F	BRINE FROM SAMPLE 23	CHLORINITY	149.12 ‰
G	BRINE FROM SAMPLE 26	CHLORINITY	161.01 ‰
H	BRINE FROM SAMPLE 29	CHLORINITY	167.49 ‰
I	BRINE FROM SAMPLE 31	CHLORINITY	174.60 ‰

Figure 11. Time temperature curves for melting of frozen sea water and various brines. (Curves are displaced to the right for zero time.)

sodium chloride dihydrate decreased in size and occurred at a lower temperature. This plateau disappeared entirely in the curve for Sample 26.

The curves for the brines of Samples 29 and 31 were obtained with a smaller volume of brine. Therefore the shapes of these curves should not be compared with the shapes of the other curves in Fig. 11. In addition to the plateau at −36.0° C, the time-temperature curve for Sample 29 had an inflection point at −54° C. Although it is not readily apparent in Fig. 11, this inflection point is discernible in a plot of the slope of the curve against the temperature.

The −54° C inflection point is easily seen in the time-temperature curve from the brine of Sample 31. This inflection point probably results from the solidification of the last of the brine. The general shape of this curve differs from the other curves because the thermal analysis was conducted in the freezer at a temperature of −30° C in order to enhance the −54° C inflection point.

DISCUSSION

Since sea water is a dilute solution of very soluble salts, a large portion of the water must be removed from the solution before any salt will begin to crystallize. Therefore, when sea water is exposed to freezing conditions, ice is the first solid phase. During the beginning of the freezing process, the freezing point of the sea water decreases slowly due to the large quantity of ice formed. Approximately 80% of the water in sea water has been transformed into ice before the first salt crystallizes from the resulting brine at −8.2° C. The concentrations of the six major ions increase until the freezing point reaches −8.2° C.

In addition to the continued formation of ice, crystals of sodium sulfate decahydrate begin to appear at −8.2° C. The concentration of sulfate decreases markedly as the freezing point continues downward. For the other ions in the brine, there is an increase in concentration in the interval from −8.2 to −22.9° C. The sodium sulfate decahydrate crystals form mainly on the bottom of the container, a few adhering to the under surface of the ice. The habit of the monoclinic crystals consists of well-formed columns, elongated tablets, and short prisms. Upon exposure to air, the crystals effloresce rapidly.

When the temperature reaches −22.9° C, the amount of brine remaining is only about 2% of the initial quantity of sea water. From this concentrated brine, sodium chloride dihydrate precipitates as the temperature decreases below −22.9° C. The monoclinic crystals of sodium chloride dihydrate form initially as white spherulites on the bottom and lower walls of the vessel, and as the temperature decreases

they increase in size and number; in addition, they begin to form on the under surface of the ice. The spherulites, which eventually grow together into large masses of crystals in the bottom portion of the container, also begin to form throughout the ice. Most of the ice eventually has a white color due to crystals of sodium chloride dihydrate. The sodium concentration in the brine shows a marked decrease during this precipitation phenomenon. The concentrations of potassium, magnesium, calcium and chloride in the brine continue to increase as the temperature approaches −36.0° C. Upon isolation from the brine, the crystals of sodium chloride dihydrate melt at 0.2° C to form crystals of sodium chloride and a saturated solution of the salt.

Below −36.0° C, the concentrations of magnesium and potassium in the brine decrease. The thermal analysis studies show that a salt begins to precipitate at −36.0° C. Since the salt melted when the temperature increased, reliable optical identifications could not be made.

When the concentrations of sulfate in the brines are low, the brines are mainly aqueous solutions of the chlorides of sodium, potassium, calcium and magnesium. An inspection of the potassium chloride-magnesium chloride-water system shows that carnallite forms only from magnesium chloride rich solutions above −21° C. Below this temperature, potassium chloride and magnesium chloride dodecahydrate precipitate instead of carnallite. The system is scarcely changed by the addition of sodium chloride. Likewise, low concentrations of calcium chloride will not alter the system very much. From available information and an examination of the simpler salt systems, the salt forming at −36.0° C is a mixture of two single salts, potassium chloride and magnesium chloride dodecahydrate, rather than the double salt, carnallite.

The inflection points at −54° C in the time-temperature curves for the brines of Samples 29 and 31 are probably due to the formation of calcium chloride hexahydrate. This is the only calcium-containing salt formed at low temperatures in the various systems composed of water and the chlorides of calcium, sodium and magnesium. The last of the brine, which is rich in calcium chloride, solidifies at a temperature probably only slightly below −54° C.

Literature Cited

Chamot, E. M. and C. W. Mason
1948. Handbook of Chemical Microscopy. Volume II. John Wiley and Sons, New York. 438 pp.

D'Ans, J.
1933. Die Losungsgleichgewichte der Systeme der Salze ozeanischer Salzablagerungen. Verlagsgesellschaft fur Ackerbau m. b. H., Berlin. xii + 807 pp.

Phillips, F. C.
1947. Oceanic salt deposits. Quart. Rev. (London), *1:* 91–111.
Ringer, W. E.
1906. De veranderingen in samenstelling van zeewater bij het bevriezen. Chem. Weekbl., *3:* 223–249.
Thompson, T. G.
1932. The physical properties of sea water. Bull. nat. Res. Coun., Wash., No. 85: 84.
Thompson, T. G., W. R. Johnston, and H. E. Wirth
1931. The sulfate-chlorinity ratio in ocean waters. J. Cons. int. Explor. Mer, *6:* 246–251.
Usiglio, M. J.
1849. Analyse de l'eau de la Mediterraneane sur le Cotes de France. Annales de Chimie et de Physique, *27:* series 3, 92–107, 172–191.
van't Hoff, J. H.
1905, 1909. Zur Bildung der ozeanischer Salzablagerungen. Parts I and II. Brunswick, 1905: 6 + 85 pp.; 1909: 6 + 90 pp.
1912. Untersuchungen über die bildungsverhält nisse ozeanischer salzablagerungen. Leipzig, 10+ 91 pp.

IRON IN MARINE WATERS[1]

By

GEORGE J. LEWIS, JR. and EDWARD D. GOLDBERG

University of California, Scripps Institution of Oceanography
La Jolla, California

ABSTRACT

The soluble and particulate iron in marine waters of the North Pacific were determined spectrophotometrically by utilizing the iron complexes of alpha, alpha-bipyridyl and bathophenanthroline. Particulate iron is defined as that iron which was retained by a molecular filter, the soluble iron as that which passed through the molecular filter. The soluble iron in surface and deep waters varied but slightly about 3.4 g/L. The particulate iron gave a value of 4.5 g/L. in waters deeper than 500 m, but in shoaler depths it was oftimes higher and showed a large amount of scatter. The high surface values are related to the turnover of iron by the members of the marine biosphere.

INTRODUCTION

The iron in marine waters is intimately involved in two of the primary problems of oceanography, sedimentation and productivity. Although thousands of analyses on iron have been published (Table I), a number of questions concerning its biogeochemical cycle and the results thereof remain unanswered. Analyses in the deep sea have been rare; only four out of 39 investigators have obtained samples from depths greater than 1,000 m. This is rather appalling since more than 90% of the oceanic waters lie deeper than 1,000 m.

Cooper (1948) catalogued ten forms of iron within sea water. Experimentally, however, it is difficult to quantitatively assay more than two forms, the soluble and particulate iron. Further, the distinction between these two types is arbitrarily dependent upon the porosity of the filter utilized for the separation.

With the recent availability of membrane filters (Goldberg, Baker and Fox, 1952) which rapidly pass water through their pores and which have a known porosity, it has become possible to delimit "particulate iron" by particle size. With the "Millipore Type HA" filters used in this investigation, iron particles 0.5 μ or greater were retained on the membrane; these will be designated as "particulate iron." The iron not retained by the filter will be classified as "soluble iron."

[1] Contribution of the Scripps Institution of Occanography, University of California, New Series, No. 714.

The influence of growth processes on the seasonal distribution of iron in the oceans has been observed in only one investigation (Thompson and Bremner, 1935). The fact that plankton utilize only particulate iron (Goldberg, 1952; Allen and Nelson, 1910; Harvey, 1937) focuses attention on the solid phases of iron in the sea.

In order to investigate the distribution of iron in deeper oceanic water as well as in the upper layers, analyses for particulate iron have been made for a number of stations in the northern Pacific Ocean. Since most of the iron in the sea is particulate, the inhomogeneity of the distribution invites a statistical analysis of the data.

ANALYTICAL METHODS

Two reagents, each involving the formation of an intensely red-colored complex with ferrous iron, are well suited to an analysis of iron in marine waters. α, α-bipyridyl was initially used by Cooper (1937) in an investigation of iron in English Channel waters; a modification

TABLE I. Iron Determination in Marine Waters

	Location	*Method*	*Depth (meters)*	*Fe in mg/L Soluble*	*Total*
	Northeast Atlantic				
1.*	Mediterranean	Vol. a.	I	—	2.0
2.	English Channel	?	?	—	0.10
3.	Irish Sea	Vol. a.	?	—	3.25
4.	English Channel	Col. a.	70	—	0.10
5.	English Channel	?	0–68	0.003 –0.006	—
6.	Tropical N. Atlantic (Meteor Profiles 12, 13, 14)	?	—	—	0.06
7.	Norwegian Sea	Col. b.	0–400	0.0049	0.0085
8.	Barents Sea	Col. b.	?	—	0.010–0.020
9.	North Atlantic	Col. b.	?	—	0.003–0.011 (Surface 0.013–0.014 (Bottom)
10.	English Channel	Col. c.	0–70	0.007	0.014
11.	Swedish Coast	Spectr.	?	—	0.008
12.	English Channel	Col. d.	0–120	0.000	0.020
	Northwest Atlantic				
13.	Gulf of Maine	Col. b.	1–340	—	0.019
14.	U. S. Coast	Col. b.	0–3830	0.005	0.021
15.	U. S. Coast	Col. e.	Surface	0.003	—

* See page 185 for references used in this table.

TABLE I—Continued

	Location	Method	Depth (meters)	Fe in mg/L Soluble	Fe in mg/L Total
	Northeast Pacific				
16.	Washington Coast	Col. b.	0–300	—	0.073
17.	Coasts of U. S. A., Canada, Alaska	Col. b.	0–2000	0.026	0.091
	Northwest Pacific				
18.	Seto Inland Sea	?	0–27	—	0.145
19.	Ryukyu Island	?	0–200	—	0.138
20.	Osaka-Wan Inland Sea	?	0–65	—	0.060
21.	Osaka-Wan, Osaka	?	0–10	—	0.083
22.	Seto-Naikai (Inland Sea)	?	0–150	—	0.333
23.	Kyushu Island	?	0–100	—	0.146
24.	Osaka-Wan	?	0–16	—	0.089
25.	Saruga-Wan, Honshu, Japan	?	0–978	—	0.027
26.	Osaka-Wan, Osaka	?	0–7	—	0.372
27.	Osaka Bay (off Osaka)	?	Surface	—	0.091
28.	Seto Inland Sea	?	0–33	—	0.046
29.	East China Sea (Kyushu Inlets)	?	0–68	—	0.024
30.	Sea of Japan (Fukuoka, Kyushu)	?	0–20	—	0.009
31.	Sea of Japan (Maizura Bay, Honshu)	?	0–30	—	0.212
32.	Southern Japan (Open Ocean)	?	0–1009	—	0.010
33.	Southern Japan (Osaka Bay, Kii Suido)	?	0–75	—	0.033
34.	Southern Japan (Kii Suido)	?	0–70	—	0.009
35.	Seto Inland Sea	?	0–49	—	0.069
36.	Northern Japan (Muroran Harbor, Hokkaido)	Col. b.	0–12.5	—	0.810
37.	Northern Japan (Muroran Harbor, Hokkaido)	Col. b.	0–12.5	—	0.310
38.	Off SE. Honshu and S. Shikoku	Col. d.	0–1554	—	0.0095
	All Oceans				
39.		?	?	—	1.5

Methods: Vol. a. Titration with $KMnO_4$ after $CaCO_3$ or Mg $(OH)_2$ precipitation. Col. a. Ferrocyanide development with ferric iron. Col. b. Thiocyanate development with ferric iron. Col. c. Tripyridyl development with ferrous iron. Col. d. Bipyridyl development with ferrous iron. Col. e. o-phenanthroline development with ferrous iron.

References: **1.** Usiglio, J., 1849, Ann. Chim. (Phys.), *27:* 92–107. **2.** Marchand, E., 1855, Mem. Acad. Med. (Paris), *19:* 121–318. **3.** Thorpe, T. E. and E. H. Morton, 1871, Ann. Chem. Pharmacie, *158:* 122–131. **4.** Orton, J. H., 1924, Fishery Investigations (London), (2) *6:* No. 3. **5.** Harvey, H. W., 1925, J. Mar. biol. Ass., U. K., *13:* 953–969. **6.** Wattenberg, H., 1927, Z. Ges. Erdk. Berl., No. 5–6: 307–315. **7.** Braarud, T. and A. Klem, 1931, Hvalrad. Skr., Oslo, No. 1: 1–88.

8. Bruevich, S. V., 1931, Gosudarstvennyi Okeanographficheckii Instut, Moscow, No. 1: 1–48. **9.** Bruevich, S. V., 1933, Methods of chemical oceanography, State Oceanographical Institute, Moscow, 126–129. **10.** Cooper, L. H. N., 1935, Proc. roy. Soc., *118:* 419–438. **11.** Noddack, I and W., 1940, Arkiv. Zool., *32A:* 1–35. **12.** Cooper, L. H. N., 1948, J. Mar. biol. Ass., U. K., *27:* 279–313. **13.** Seiwell, G. E., 1935, Ecology, *16:* 663–664. **14.** Rakestraw, N. W., H. E. Mahncke, and E. F. Beach, 1936, Industr. Engng. Chem. (Anal.), *8:* 136–138. **15.** Simons, L. H., P. H. Monaghan, and M. S. Taggart, Jr., 1953, Analyt. Chem., *25:* 989–990. **16.** Thompson, T. G., R. W. Bremner, and M. Jamieson, 1932, Industr. Engng. Chem. (Anal.), *4:* 288–290. **17.** Thompson, T. G. and R. W. Bremner, 1935, J. Cons. int. Explor. Mer., *10:* 39–47. **18.** Anonymous (a), 1935, J. Oceanogr., Kobe, *8:* 201–212. **19.** Anonymous (b), 1936, J. Oceanogr., Kobe, *9:* 1–16. **20.** Anonymous (c), 1936, J. Oceanogr., Kobe, *8:* 265–312. **21.** Anonymous (d), 1937, J. Oceanogr., Kobe, *10:* 1–44. **22.** Anonymous (e), 1937, J. Oceanogr., Kobe, *10:* 45–76. **23.** Anonymous (f), 1938, J. Oceanogr., Kobe, *11:* 535–610. **24.** Anonymous (g), 1939, J. Oceanogr., Kobe, *12:* 79–88. **25.** Anonymous (h), 1939, J. Oceanogr., Kobe, *12:* 37–71. **26.** Anonymous (i), 1940, J. Oceanogr., Kobe, *12:* 235–258. **27.** Yanagizawa, T., 1940, J. Oceanogr., Kobe, *12:* 435–444. **28.** Anonymous (j), 1940, J. Oceanogr., Kobe, *12:* 175–234. **29.** Anonymous (k), 1941, J. Oceanogr., Kobe, *13:* 211–285. **30.** Anonymous (l), 1942, J. Oceanogr., Kobe, *13:* 481–548. **31.** Anonymous (m), 1950, Res. mar. Obsns., Tokyo, *2:* 71–76. **32.** Anonymous (n), 1951, Res. mar. Obsns., Tokyo, *6:* 52–56. **33.** Anonymous (o), 1951, Res. mar. Obsns., Tokyo, *5:* 40–47. **34.** Anonymous (p), 1951, Res. mar. Obsns., Tokyo, *3:* 50–55. **35.** Anonymous (q), 1951, Res. mar. Obsns., Tokyo, *4:* 80–85. **36.** Tanita, S., K. Kato, and T. Okuda, 1951 (a), Bull. Faculty Fisheries, Hokkaido Univ., *1:* 66–75. **37.** Tanita, S., K. Kato and T. Okuda, 1951 (b), Bull. Faculty Fisheries, Hokkaido Univ., *2:* 220–230. **38.** Kawamoto. Takeo, 1952, Sea and Sky, *29:* 112–116. **39.** Schmidt, Carl, 1874, Bull. Acad. Sci. St. Petersb., *9:* 175–229; 1877, Bull. Acad. Sci. St. Petersb., *10:* 525–628.

of this method was adopted for our spectrophotometric determinations where quantities between 0 and 100 γ per sample were encountered. The procedure is simple and rapid, but the probable error becomes large for samples containing less than 5 γ. The colored complex is stable for at least a year in the pH range of 2.0 to 7.0.

Bathophenanthroline (4, 7-diphenyl 1, 10-phenanthroline) was used for analyses of iron samples in the concentration range below the sensitivity of bipyridyl. The method was first described by Smith, et al. (1952) for the determination of iron in raw and treated municipal water supplies and later by Peterson (1953) for the determination of serum iron. Although the method is more laborious than the bipyridyl procedure because of an extraction of the ferroin complex with isoamyl alcohol, it can be used with reasonable accuracy for total quantities of iron as small as 0.30 γ.

In the determination of particulate iron, approximately one liter of sea water was filtered per sample in order to obtain on the filter

membrane a quantity adequate for use of the bipyridyl reagent. However, the soluble iron could not be readily concentrated in a simple manner, and consequently it was necessary to use the more sensitive bathophenanthroline method.

Comparison of α, α-bipyridyl and bathophenanthroline was made by analyzing ten different samples of particulate iron by both methods. For iron concentrations of 30 γ/L, the average difference in results by the two methods was 1.6 γ/L. Although the low concentration of soluble iron made it impossible to make such a direct comparison, there is no reason to believe that the soluble iron values determined by bathophenanthroline are invalid. A thorough investigation by Smith showed no interfering ions if the pH is properly adjusted. Further evidence of the adaptability of this reaction is found in the fact that the molar extinction coefficient in sea water is the same as that in distilled water.

The oxidation process for the release of particulate organic iron by perchloric acid was tested with five samples of hemin. The average recovery was 97%.

The bipyridyl method for particulate iron was adapted for routine use aboard ship. Reagent concentrations were adjusted so that 1.0 ml dispensers could be used for each reagent with the exception of $HClO_4$ which required a 5.0 ml dispenser. A transite hood containing electrical heaters specifically constructed to fit 30 ml Kjeldahl flasks was installed for the oxidation process. In the shore laboratory much less elaborate equipment suffices; Pyrex test tubes heated on a sand bath are satisfactory.

Reagents

(1) *0.001 M bathophenanthroline.* Dissolve 0.0334 g of reagent in 50 ml of ethanol and 50 ml of water.

(2) *α, α-bipyridyl.* Dissolve 0.40 g of reagent in 100 ml of 0.2 N HCl.

(3) *10% hydroxylamine hydrochloride.* Doubly recrystallized Reagent Grade salt contains traces of iron. Dissolve 10 g of this salt in 90 ml of water and add 4 ml of Reagent (1) above. Extract the ferroin complex into two successive 10 ml portions of isoamyl alcohol and repeat this process until no further red color appears with the addition of Reagent (1). This latter procedure removes the final traces of iron.

(4) *Glacial acetic acid.* Reagent Grade.

(5) *50% sodium acetate.* To 50 g of Reagent Grade salt in 50 ml of water add 2 ml of Reagent (3) and 4 ml of Reagent (1). Extract with isoamyl alcohol until a red color ceases to appear

in the alcohol layer. If copper is present, a yellow color appears in neutral or basic solution. This does not interfere in the iron determinations, but copper should be removed since it may reduce the availability of bathophenanthroline to the ferrous ion.

(6) *Isoamyl-alcohol.* Reagent Grade or redistilled Technical Grade.

(7) *1.2 N HCl.* Dilute 10 ml of concentrated Reagent Grade HCl to 100 ml.

(8) *70% perchloric acid.* Reagent Grade perchloric acid contains small quantities of iron, about 1.4×10^{-1} γ/ml. Since purification is impractical, this iron must be taken into account in the reagent blank.

(9) *Standard ferric iron solution.* To obtain a solution containing 400 γ of ferric iron/ml, dissolve 0.3455 g of $Fe(NH_4)(SO_4)_2 \cdot 12\ H_2O$ in 100 ml of iron free water with 1.6 ml of concentrated HCl added. 10 ml of this solution are diluted to 100 ml and 1000 ml to give working standards for the bipyridyl and bathophenanthroline methods respectively.

Determination of Particulate Iron with α, α -Bipyridyl

Sample Analysis. Measured samples of approximately 1.2 l, collected in Nansen bottles, were passed through a membrane filter, after which the membrane was placed in a 30 ml Vycor Kjeldahl flask containing 5 ml of perchloric acid. Heat was applied until no further evolution of acid fumes was observed. When cooled, 1 ml of 1.2 N HCl and 10 ml of water were added, after which the contents were transferred to a 50-ml glass stoppered graduated cylinder. The flask was rinsed with two 10 ml portions of water. The combined solutions were treated with 1 ml each of hydroxylamine hydrochloride, sodium acetate, and bipyridyl solutions. After the sample was diluted to 50 ml, its optical density was determined in 10 cm cells in a Beckman DU Spectrophotometer at 522 mμ.

Standardization Curves. 0.00, 0.20, 0.40, 0.60, 0.80, and 1.00 ml volumes of the standard ferric solution containing 40 γ/ml were treated with 1 ml each of 1.2 N HCl, sodium acetate, hydroxylamine and bipyridyl solutions; each solution was then diluted to volume in a 50 ml flask. The optical density was determined as above. Beer's Law curves are easily reproduced to within 2%.

Reagent Blanks. If the reagent solutions are properly purified, the only extraneous iron comes from the perchloric acid and the filter membrane. A large number of membranes from several different packages were analyzed and were found to average 2.0 γ of

iron per membrane with a standard deviation of 2.0 γ. Since there is a variation from one package to another, the reagent blank was determined for each package by assaying several pads.

Determination of Soluble Iron with Bathophenanthroline

Sample Analysis. Five ml of 70% perchloric acid were added to 100 ml of filtered sea water in a Pyrex or Vycor Kjeldahl flask, and the solution was evaporated until the sea salt formed a thin paste. Care was taken not to evaporate to bone dryness, since this gave low results, probably from the formation of difficultly-soluble iron oxides. The residue, dissolved in 100 ml of water, was heated to boiling.

After the solution cooled to room temperature, 2 ml of hydroxylamine hydrochloride were added, and the pH was adjusted to 4.0 by the addition of 0.4 ml of glacial acetic acid and 50% sodium acetate. The required quantity of sodium acetate depended upon the amount of $HClO_4$ retained in the sea salt.

Following buffering, 4.0 ml of bathophenanthroline reagent were added, and the colored complex was extracted with 20 ml of isoamyl alcohol. Two extractions with 10 ml of alcohol proved adequate. The alcohol was transferred to a 25 ml volumetric flask and diluted to volume. In most cases it was difficult to prevent a few small drops of salt water from entering the flask, but these settled to the bottom and caused no interference. The transmission was then determined in a 10 cm cell at 533 mμ.

Standardization Curves. Because the extinction coefficient of the bathophenanthroline complex is not affected by the presence of sea salt in the aqueous sample, it was not necessary to use sea water in the standardization analyses.

To 100 ml portions of water in 125 ml separatory funnels were added respectively 0.00, 0.30, 0.60, 0.90, 1.20 and 1.50 ml of a ferric iron standard containing 4.00 γ/ml. The samples were treated with 1.0 ml glacial HAc, 0.85 ml of 50% sodium acetate, 2.0 ml of 10% hydroxylamine hydrochloride, and 4.0 ml of bathophenanthroline. After extraction with two 10 ml portions of isoamyl alcohol, the extract was diluted to 25.0 ml in a volumetric flask with redistilled ethanol. The samples were read in the spectrophotometer as above.

Reagent blanks. These values were determined by evaporating 5.0 ml of 70% $HClO_4$ until only a small fraction of a milliliter remained in the flask. Subsequent processing was identical with that used for the sea water samples.

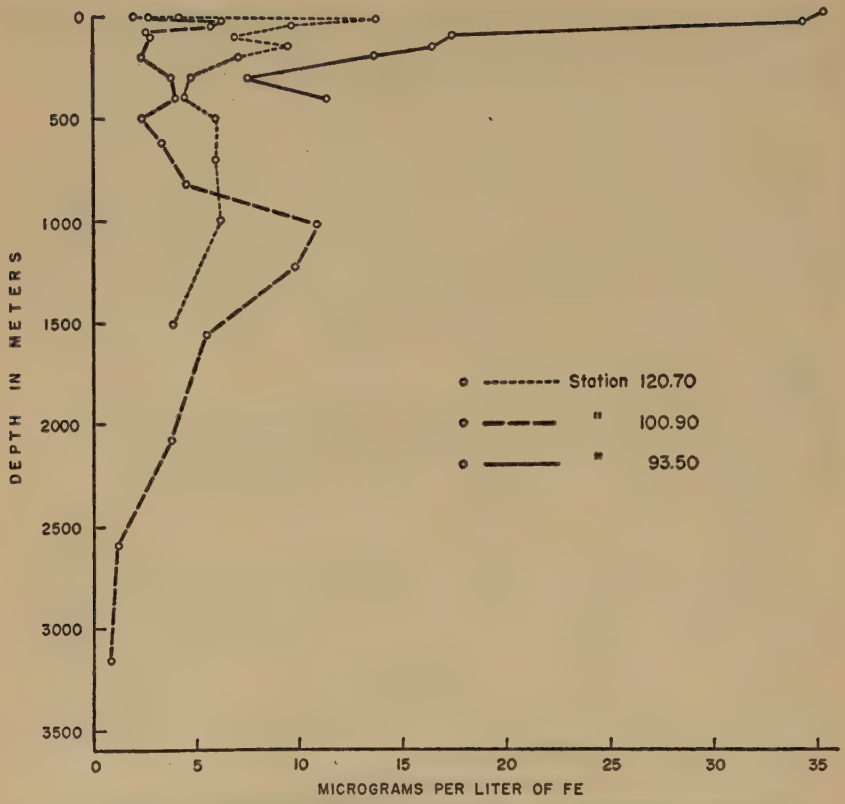

Figure 1. Vertical distribution of particulate iron off the California coast.

RESULTS

Initially, particulate iron analyses were made off the coast of California. Typical data are shown graphically in Fig. 1. The results indicated a decided concentration of iron in the upper water masses. Further, replicate analyses showed poor agreement, sometimes differing by factors as high as five. To determine whether or not this observed variation was significant and to study the variation in samples from the same depth, a set of experiments was devised to make the results amenable to statistical analysis (Dixon and Massey, 1951).

Clusters of three Nansen bottles per depth (5 m apart, the minimum safe working distance) were arranged for each station in order to study the variation at a given depth. Ten depths ranging from the surface to 3500 m were taken. Nine stations were made on the 1953

TABLE II. Iron Analyses Trans-Pacific Expedition
Particulate Iron in μg/L

Nominal Depth	Station 7	Station 12	Station 20	Station 30	Station 40	Station 47	Station 54	Station 70	Station 80
	36°21.8′N	40°26.9′N	49°29.5′N	53°57.7′N	53°57.0′N	49°50.1′N	40°34.5′N	39°44.0′N	35°04.5′N
	134°53.0′W	143°32.0′W	154°56.5′W	175°04.5′W	171°10.8′E	165°49.2′E	170°02.3′E	148°24.0′E	145°07.5′E
10	36, 37, 34	14, 10, 8	6, 6, 6	2, 5, 14	0, 3, 13	0, 0, 1	0, 4, 6	4, 0, 1	0, 5, 3
50	23, 29, 50								
100	35, 14, 28	20, 20, 16	11, 13, 11	6, 1, 3	11, 10, 15	0, 0, 0	3, 1, 14	1, 4, 0	0, 2, 0
200	27, 24, 32	15, 12, 5	17, 9, 8	5, 7, 12	7, 8, 2	0, 1, 6	0, 0, 4	1, 8, 1	3, 13, 19
300	15, 16, 31	6, 4, —	4, 1, 7	6, 9, 2	0, 0, 9	0, 0, 0	6, 0, 6	1, 2, 1	0, 0, 5
400		11 — —	10, 7, 29	3, 7, 8	6, 8, 16	3, 4, 0	4, 2, 6	1, 0, 0	0, 0, 6
500	30, 10, 11	5, 5, 3	6, 4, 5	5, 5, 6	2, 0, 11	1, 2, 0	1, 5, 0	1, 0, 9	2, 5, 2
700	13, 10, 16								
1000	14, 13, 26	5, 6, 5	3, 3, 10	4, 5, 4	0, 1, 3	2, 3, 11	3, 0, 1	0, 1, 0	2, 0, 1
1500	17, 10, 17								
2000	14, 11, 15	8, 8, 3	3, 6, 4	4, 15, 2	4, 12, 7	10, 8, 4	2, 1, 1	4, 1, 1	0, 0, 12
3000		2, 2, 4	2, 16, 2	5, 16, 7	0, 6, 17	5, 11, 14	9, 11, 5	5, 1, 2	0, 1, 0
3500		5, 9, 7	4, 6, 10	7, 5, 5	5, 3, 0	3, 1, 2	1, 1, 11	0, 0, 0	2, 0, 1

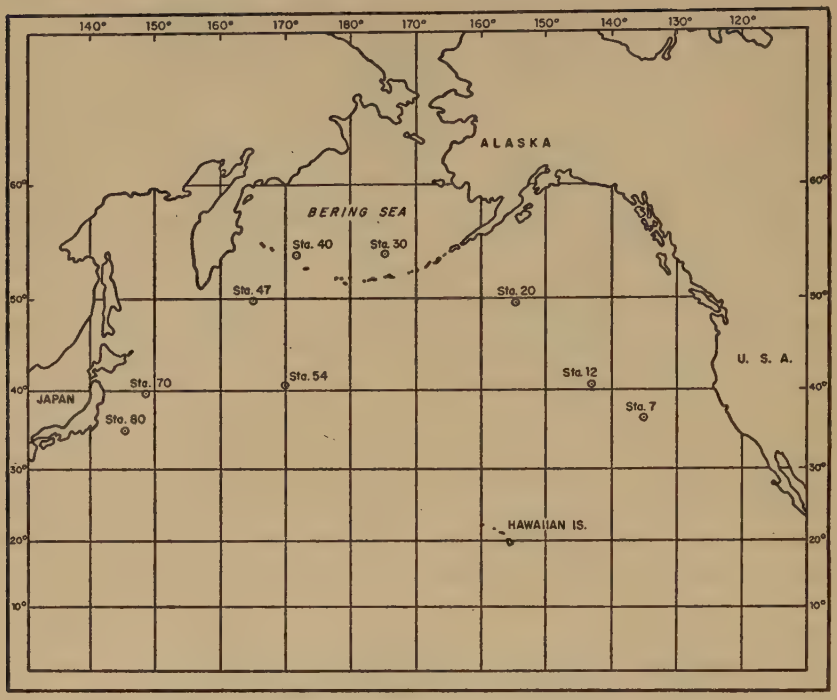

Figure 2. Station positions on the Trans-Pacific expedition of the Scripps Institution of Oceanography, 1953.

Trans-Pacific Expedition of the Scripps Institution of Oceanography (Fig. 2) (Wooster, 1954), and the results are given in Tables II and III.

An analysis of variance was made for each station to ascertain if the surface and deep populations were significantly different (Table IV). Stations 7, 12, 20 and 47 evince discrete populations at the two levels, 0 to 400 and 500 to 3500 m, whereas no statistical difference exists in the other five stations.

An intercomparison of the surface and deeper waters between stations is presented in Table V. Station 7 is markedly different from all other stations in both of its distinct populations. Station 47, with a notable absence of iron in the upper layers, appears unique. The data also emphasize the fact that the deeper waters show less variation between populations than the surface values. The analysis of variance of the iron populations for a given station shows that the variation within a cluster is as great as the variation between clusters.

TABLE III. Summary of Table II.
Particulate Iron From Trans-Pacific Stations

Station	0–400 *m* av.		500–3500 *m* av.		*Av. of all depths*	
	γ/L	*Std. Dev.*	γ/L	*Std. Dev.*	γ/L	*Std. Dev.*
7*	27	11	17	6	23	10
12	12	5	5	2	8	5
20	10	7	6	4	8	6
30	6	4	6	4	6	4
40	7	5	5	5	7	5
47	1	2	5	4	3	4
54	4	4	4	4	4	4
70	2	2	2	3	2	2
80	4	6	2	3	3	5

* Upper layer depth range 0–300 m; deep water layer 500–2000 m.

TABLE IV. Analysis of Variance for Comparison of Particulate Iron in the Upper (0–400 m) Layer with That in the Deep Water (500–3500 m). Data from Trans-Pacific Expedition.

Station		*Sums of Squares*	*Degrees of Freedom*	*Variance*	*F ratio*
7*	Between Layers	1526	1	1526	24.2
	Within Layers	1761	28	63	
12	Between Layers	293	1	293	18.7
	Within Layers	393	25	16	
20	Between Layers	124	1	124	4.27
	Within Layers	813	28	29	
30	Between Layers	1	1	1	0.07
	Within Layers	409	28	15	
40	Between Layers	51	1	51	1.82
	Within Layers	785	28	28	
47	Between Layers	136	1	136	11.5
	Within Layers	328	28	12	
54	Between Layers	0.2	1	0.2	0.01
	Within Layers	407	28	15	
70	Between Layers	0.2	1	0.2	0.04
	Within Layers	158	28	5.6	
80	Between Layers	26	1	26	1.29
	Within Layers	566	28	20	

* Upper layer depth range 0–300 m; deep water layer 500–2000 m. Critical F_{99}—7.64 except for Station 12, where F_{99} is 7.82. Critical F_{95}—4.20 except for Station 12, where F_{95} is 4.26.

Eight samples of water collected from the Scripps Pier at La Jolla as well as duplicate samples of bottom water collected from two locations in the open Pacific Ocean were passed through a molecular filter for an analysis of the soluble iron. The results are given in

TABLE V. F Ratios for Intercomparison of Trans-Pacific Expedition Stations

Upper Layer (0–400 m)

Station	*12*	*20*	*30*	*40*	*47*	*54*	*70*	*80*
7*	32	40	78	61	126	93	105	80
12	—	0.8	11	4.7	50	21	43	14
20	—	—	3.5	1.3	25	9.2	20	7.1
30	—	—	—	0.5	22	2.8	15	1.7
40	—	—	—	—	18	4.2	13	3.0
47	—	—	—	—	—	7.3	1.5	3.9
54	—	—	—	—	—	—	3.5	0.0
70	—	—	—	—	—	—	—	1.8
80	—	—	—	—	—	—	—	—

Deep Water (500–3500 m)

7*	39	24	24	27	28	42	65	60
12	—	0.1	1.1	0.1	0.0	2.0	16	11
20	—	—	0.3	0.3	0.1	2.2	11	6.0
30	—	—	—	1.0	0.8	4.0	15	11.9
40	—	—	—	—	4.1	0.6	4.2	3.3
47	—	—	—	—	—	0.9	6.0	4.7
54	—	—	—	—	—	—	2.2	1.5
70	—	—	—	—	—	—	—	0.1

* Upper layer 0–300 m; Deep water 500–2000 m. F_{99} critical values are 7.64 for all station comparisons except those involving Station 12, in which case F_{99} is 7.82. F_{95} critical values are 4.20 for all station comparisons except those involving Station 12, in which case F_{95} is 4.26.

TABLE VI. Soluble Iron Content of Sea Water

Sea Water Sample	*γ/L Soluble Iron*
La Jolla, California	4.1
	4.1
	3.6
	2.0
	3.3
	5.2
	3.3
	0.7
Mean	3.3
Bottom Water (4000 m) 12°S; 129°W.	2.6, 5.5
Bottom Water (4500 m) 11°S; 134°W.	2.6, 3.9
Mean	3.7
Grand Mean	3.4

Table VI. Mean values for the two groups of samples are 3.3 and 3.7 μg/L respectively, with an over-all average of 3.4 μg/L. This compares favorably with the soluble iron concentrations found previously as given in Table I with the exception of the 1935 value obtained by Thompson and co-workers.

DISCUSSION

The concentration of iron in the characteristic deep water of the North Pacific approximates 8 μg/L, with slightly greater than half of that value being contributed by the particulate iron (4.5 μg/L). This value, though lower than the previously accepted values, is in accord with the only other reported value which includes the deeper water of the Pacific (Table I, ref. no. 32).

Soluble iron values are far greater than those that can be accounted for by ionic iron at equilibrium with the constituents of sea water at a pH of 8. This value was shown by Cooper (1937) to be not more than 5×10^{-8} μg/L. The ferrifluoride complex ion FeF_6^{---} has been suggested by Thompson, et al. (1932) as a form of soluble iron in sea water, but Cooper (1948) has shown empirically that it is thermodynamically unstable. It is likely that the soluble iron found in this and other investigations consists of dissolved or colloidal organic compounds which arise from the marine biosphere; likely it also consists of the colloidal inorganic compounds such as ferric hydroxide and ferric phosphate. These colloidal species are of such dimensions that they pass through filters of approximately 0.5 micra porosity. Furthermore, these forms are quite uniformly dispersed throughout the oceans, evidence for which is found in the agreement between samples from deep and coastal waters and between the results of this work and that of previous investigators.

The occurrence of two populations of particulate iron in the three easternmost stations of the Trans-Pacific Expedition (Stations 7, 12, 20) and in the earlier California coastal work is probably related to the activity of the inhabitants of the marine biosphere. The accumulation of particulate iron by diatoms is followed by either the death of the organism or the uptake of the organism by higher members of the food chain. Inasmuch as many of the latter organisms are involved in the vertical migrations of zooplankton, defecation and mortality by this group together with concurrent re-uptake of the discarded matter result in the cycling of iron in the upper water layers. Thus, the marine biosphere acts as a reservoir for iron particles and accentuates the high scatter of the particulate iron distribution. Relative homogeneity of particulate iron content reflects low biological activity or high rates of mixing of waters.

SUMMARY

1. It is feasible experimentally to differentiate the iron in marine waters into two classes: "particulate iron" which is retained on a molecular filter and "soluble iron" which passes through the molecular filter.

2. In the northern Pacific the soluble iron in surface and deep waters shows values varying but slightly about 3.4 μg/L.

3. The particulate iron in waters deeper than 500 m averages 4.5 μg/L whereas in shoaler waters the values are ofttimes higher and show a larger amount of scatter. For some stations in the North Pacific the upper and lower iron concentrations, as determined from analyses of variance upon the data, are significantly different.

4. High values of iron in surface waters are attributed to the turnover of iron within the marine biosphere. As a result of the interaction between biosphere and hydrosphere with respect to iron, the upper waters act as a reservoir for iron.

REFERENCES

Allen, E. J. and E. W. Nelson
1910. On the artificial culture of marine plankton organisms. J. Mar. biol. Ass., U. K., *8:* 421–474.

Cooper, L. H. N.
1937. Some conditions governing the solubility of iron. Proc. roy. Soc., *124:* 299–307.
1948. The distribution of iron in the waters of the western English Channel. J. Mar. biol. Ass., U. K., *27:* 279–313.

Dixon, W. J. and F. J. Massey
1951. Introduction to statistical analysis. McGraw-Hill Book Co., New York. 370 pp.

Goldberg, E. D.
1952. Iron assimilation by marine diatoms. Biol. Bull., Woods Hole, *102:* 243–248.

Goldberg, E. D., Marjorie Baker, and D. L. Fox
1952. Microfiltration in oceanographic research. I. Marine sampling with the molecular filter. J. Mar. Res., *11* (2): 194–204.

Harvey, H. W.
1937. The supply of iron to diatoms. J. Mar. biol. Ass., U. K., *22:* 205–219.

Peterson, R. E.
1953. Improved spectrophotometric procedure for determination of serum iron. Analyt. Chem., *25:* 1337–1339.

Smith, G. F., W. H. McCurdy, Jr., and H. Diehl
1952. The colorimetric determination of iron in raw and treated municipal water supplies by use of 4 : 7—Diphenyl—1 : 10—phenanthroline. Analyst, *77:* 418–422.

Thompson, T. G. and R. W. Bremner
1935. The occurrence of iron in the waters of the Northeast Pacific Ocean. J. Cons. int. Explor. Mer., *10:* 39–47.
Thompson, T. G., R. W. Bremner and M. Jamieson
1932. Occurrence and determination of iron in sea water. Industr. Engng. Chem. (Anal.), *4:* 288–290.
Wooster, W. S.
1954. Recent oceanographic exploration in the North and Equatorial Pacific Ocean. Proc. 8th Pacif. Sci. Congr. (in press).

STATISTICS OF THE SEA SURFACE DERIVED FROM SUN GLITTER[1]

By

CHARLES COX AND WALTER MUNK

Scripps Institution of Oceanography

ABSTRACT

Aerial photographs of the sun's glitter on the sea surface, taken under carefully chosen conditions in the Hawaiian area, were coordinated with measurements of winds (1–27 knots) from a vessel. Statistics of the glitter, interpreted in terms of the statistics of the slope distribution of the sea surface, gave the following results: (1) As a first approximation the slope distribution is found to be Gaussian; this can be accounted for by an arbitrarily wide *continuous* spectrum of ocean waves, but not by a spectrum consisting of a few discrete frequencies. (2) The ratio of the up/down-wind to crosswind components in mean square slope is less than two; this indicates a directional "beam width" in excess of 130° for the relatively short waves that contribute to the slope spectrum. (3) The mean square slope, regardless of direction, increases linearly with wind speed and reaches a value of $(\tan 16°)^2$ for a wind speed of 14 m sec^{-1}; this empirical relation follows in form and to an order of magnitude from a spectrum proposed by Neumann on the basis of wave amplitude observations. A spectrum proposed by Darbyshire cannot be reconciled with our observations.

Further results which have not been interpreted are: (4) An up- and down-wind skewness which increases with increasing wind speed is such as to make the most probable slope a few degrees rather than zero, with the azimuth of ascent pointing downwind. (5) A peakedness, which is barely above the limit of observational error, is such as to make the probability of very large and very small slopes greater than Gaussian. (6) Oil slicks laid by the vessel over an area of one quarter square mile reduce the mean square slope by a factor of two or three and eliminate skewness but leave peakedness unchanged.

The distribution of particle acceleration is closely related to the distribution of slope. Accordingly, the total mean square acceleration increases linearly with wind speed and reaches a value (at the surface) of $(0.4\ g)^2$ at a wind speed of 14 m sec^{-1}.

1. INTRODUCTION

If the sea surface were absolutely calm, a single mirror-like reflection of the sun would be seen at the *horizontal specular point.* In the usual case there are thousands of "dancing" highlights. At each highlight there must be a water facet, possibly quite small, which is so inclined

[1] Contribution from the Scripps Institution of Oceanography, New Series, No. 731. This work has been sponsored by the Geophysics Research Directorate of the Air Force Cambridge Research Center, under Contract No. AF 19(122)–413.

as to reflect an incoming ray from the sun toward the observer. The farther the facet is from the horizontal specular point, the larger must be its slope in order to reflect the sun's rays back to the observer. The distribution in the glitter pattern is therefore closely related to the distribution of surface slopes.

In order to exploit this relationship, plans were laid in 1951 for coordination of aerial photographs of glitter from a B-17G plane with meteorological measurements from a 58-foot schooner, the REVERIE. The first measurements were made in July 1951 offshore from Monterey, California, where a variety of wind conditions could be expected. But one of the requirements for photographing the sun's glitter is sunshine. Unfortunately the number of clear days was even fewer than those given on climatological charts, hence only two successful flights were completed. Accordingly, plane and vessel were moved to Hawaii, where one can select radically different wind conditions by moving short distances. The island of Maui was chosen because the region surrounding this island is the least clouded in the Hawaiian area. Also, the harbor and airport facilities are conveniently near to one another. Conditions were excellent, and all observations were taken during the period 25 August to 25 September 1951.

Since the air borne instrumentation has been described by Cox and Munk (1954), we shall limit ourselves to a few comments on measurements from the vessel. Bendix Friez Aerovane anemometers were installed on the fore masthead (41 ft) and bowsprit (9 ft) of the REVERIE. At the time the aerial photographs were taken, the vessel would heave to, with the wind abeam, and be steadied by sails. With this arrangement the error inherent in using cup-type anemometers on a rolling vessel can be avoided. The output of the masthead anemometer and the difference between that and the bowsprit anemometer were smoothed by an R, C-filter with 18-second time constant and were recorded on two Esterline-Angus milliammeters. Wind direction was estimated by eye. For some of the earlier measurements we attempted to raise and lower a hand anemometer with the movement of boat and waves so as to keep it 3 ft above the water surface. Other measurements included air and water temperatures, and wet and dry bulb temperatures.

One of the objects of this investigation was a study of the effect of surface slicks. Early attempts to spray powdered Atco-grain detergent from vessel or plane were unsatisfactory. In the method adopted, oil was pumped on the water, the mixture consisting of 40% used crank case oil, 40% diesel oil, and 20% fish oil. With 200 gallons of this mixture, a coherent slick 2000 by 2000 ft could be laid in 25 minutes, provided the wind did not exceed 20 mph.

2. METHOD

Here we limit ourselves to a brief review of the method, since a full discussion is given by Cox and Munk (1954). Two pairs of aerial cameras, mounted in the plane, were wired for synchronous exposure. Each pair consisted of one vertical and one tilted camera with some overlap in their fields of view. One pair gave ordinary *image* photographs for the purpose of locating cloud shadows, slicks, and vessel; this pair also gave the positions of the horizon and the plane's shadow (to correct for the roll, pitch and yaw of the plane). The other pair of cameras, with lenses removed, provided *photometric* photographs. Sample photographs are shown in Figs. 1 and 2.

The method consists essentially of two phases. The first identifies, from geometric considerations, a point on the sea surface (as it appears on the photographs) with the particular slope required at this point for the reflection of sunlight into the camera. This is done by suitable grid overlays (see Figs. 1 and 2). Lines of constant α (radial) give the azimuth of ascent to the right of the sun; lines of constant β (closed curves) give the tilt in degrees. The grids depend on the elevation ϕ of the sun and on the orientation of the camera but not on the height of the camera. The effect of the setting sun is to concentrate the pattern along a narrow street (Fig. 1).

The second phase interprets the average brightness of the sea surface (darkening on the photometric negative) at various α,β-intersections in terms of the frequency with which this particular slope occurs. At the horizontal specular point the sea surface is apt to be so bright as to be blinding to the eye, whereas at some distance from this point the surface is much darker. The principal reason for this variation is that the gentle slopes (required for highlights near the horizontal specular point) occur more frequently than steep slopes. On the *density photographs* the glitter pattern appears as a round blob with a bright core (on the positive print) and a gradually diminishing intensity to the outside (Fig. 1, lower right). The density, D, of the blob on the negative is then measured with a densitometer at points which correspond to the intersection of appropriate grid lines. Factors other than the slope probability enter into the problem and have to be allowed for.

In addition to the reflection of the sun's rays from the sea surface, there are two other distinct sources of radiation: (1) the skylight reflected at the sea surface, and (2) the sunlight scattered by particles beneath the sea surface. We have attempted to correct for these. The disappearance of the glitter into this background imposes the essential limitation on the determination of the probability of large (and infrequent) slopes.

3. RESULTS

The results of these measurements are tabulated values of slope probability for various values of α,β. Instead of presenting these tabulated values we achieve compactness by giving the results in analytical form as a function of wind speed, thus bringing out the essential physical content. In this way the experimental error is also subdued. A reasonable approach is to make use of the fact that the distribution is close to Gaussian. By representing the data as a Gram-Charlier series we can develop the deviations from the normal distribution in a systematic manner. These deviations represent skewness and peakedness and therefore have a simple physical interpretation.

Some notation has to be introduced. Let x designate the crosswind coordinate, y the upwind coordinate, and z the elevation of the surface; furthermore, let β be the tilt and $m = \tan\beta$ the slope (regardless of direction) of a small element of sea surface, and let α be its azimuth of ascent to the right of the *wind* (not of the sun, as before). Then

$$z_x = \partial z/\partial x = m \sin\alpha, \qquad z_y = \partial z/\partial y = m\cos\alpha \tag{1}$$

are the crosswind and upwind components of slope. Since the mean sea level is nearly horizontal over large distances, it follows that the mean values of z_x, z_y (averaged over many waves) are zero. However, the mean values of z_x^2, z_y^2 do not vanish and will be designated by σ_c^2, σ_u^2. Hence σ_c, σ_u are the crosswind and upwind rms slope components. The corresponding "standardized" components are defined by

$$\xi = z_x/\sigma_c, \qquad \eta = z_y/\sigma_c\,. \tag{2}$$

Now let p be the probability of slopes. More precisely, let

$$p\,dz_x\,dz_y; \quad p\,m\,d\alpha\,dm; \quad p\tan\beta\sec^2\beta\,d\alpha\,d\beta$$

designate the probabilities that the slopes lie within the limits

$$z_x \pm \tfrac{1}{2}dz_x,\ z_y \pm \tfrac{1}{2}dz_y; \quad \alpha \pm \tfrac{1}{2}d\alpha,\ m \pm \tfrac{1}{2}dm; \quad \alpha \pm \tfrac{1}{2}d\alpha,\ \beta \pm \tfrac{1}{2}d\beta.$$

Which of these three equivalent forms is convenient depends on the particular problem under consideration. Our measurements show that p can be adequately represented by the expression

$$\begin{aligned} p = (2\pi\sigma_c\sigma_u)^{-1}\exp\left[-\frac{1}{2}(\xi^2+\eta^2)\right]\Big\{1 &- \frac{1}{2}c_{21}(\xi^2-1) \\ &- \frac{1}{6}c_{03}(\eta^3-3\eta) + \frac{1}{24}c_{40}(\xi^4-6\xi^2+3) \\ &+ \frac{1}{4}c_{22}(\xi^2-1)(\eta^2-1) + \frac{1}{24}c_{04}(\eta^4-6\eta^2+3)\Big\} \end{aligned} \tag{3}$$

for slopes up to $\xi = \eta = 2.5$.

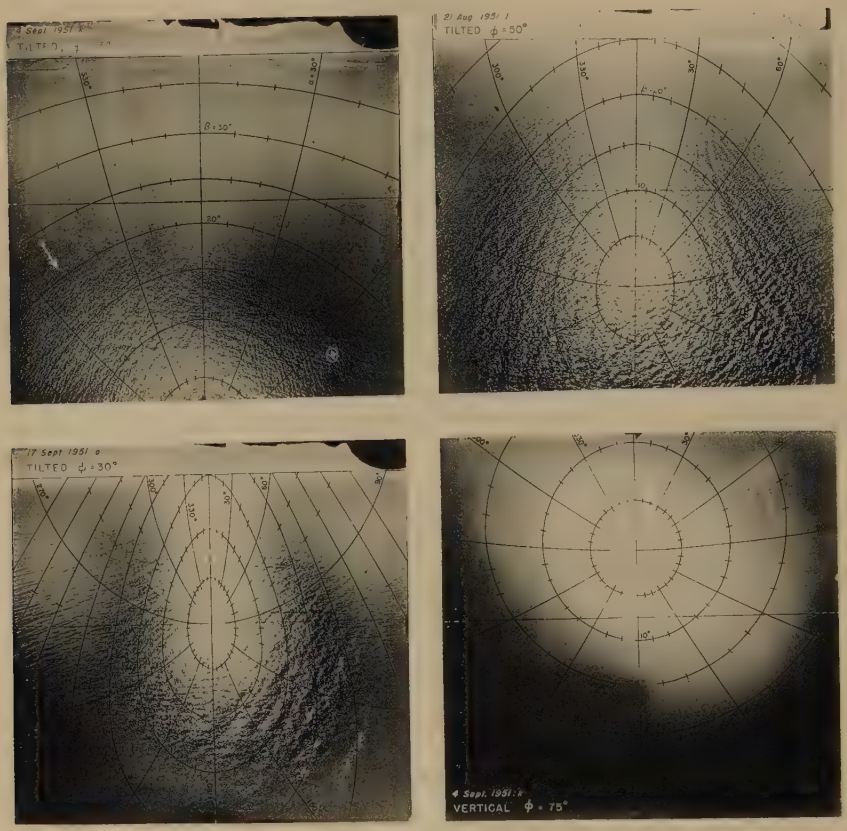

Figure 1. Upper Left and Right and Lower Left: The glitter pattern at solar elevations of $\phi = 75°$, 50° and 10° respectively. The superimposed grids consist of lines of constant slope azimuth α (radial) drawn for every 30° and of constant tilt β (quasi-elliptical) for every 5°. The vessel Reverie is encircled in upper left photograph. The white arrow indicates wind direction. Lower Right: Photometric photograph. Broken arrow indicates light circle due to Reverie.

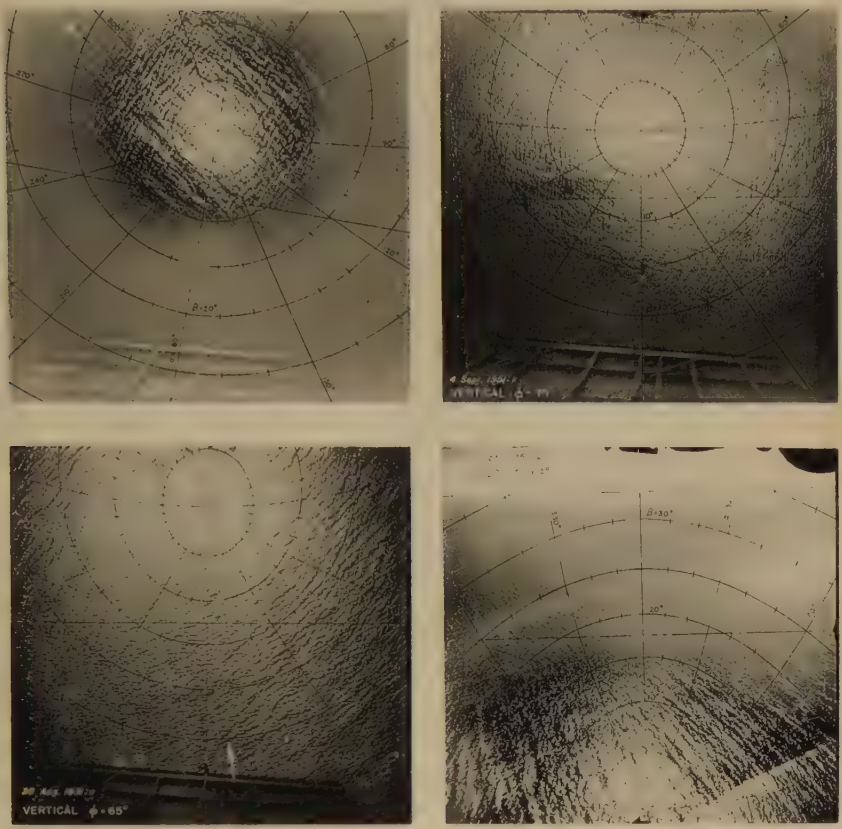

Figure 2. Upper Left and Right and Lower Left: The glitter pattern at wind speeds of 0.7, 3.9 and 14 m s^{-1} respectively. Large rotation of grid in upper left photograph is due to bad yaw as indicated by off-center position of plane's shadow (within white cross). Lower Right: A rectangular artificial slick, with near boundary almost through specular point. Brightness of slick sea surface is reduced for large β and somewhat increased for small β.

TABLE I

*Photograph Designation**	*Time†*	*Location of cameras*		*Wind*			*Temp. (°C) Sea Surface*
		N. Lat.	*W. Long.*	*Speed ms⁻¹*		*Direction*	
				41 ft#	*9 ft#*	*(true)*	
28 Aug. b	1106	21°01.8′	156°45.8′	11.6	9.6	060°	26.15°
28 Aug. p	1336	20°59.0′	156°44.0′	13.3	11.0	050°	26.4°
28 Aug. u	1403	20°58.2′	156°43.3′	13.8	11.6	050°	26.3
28 Aug. v	1403	20°58.2′	156°43.3′	13.7	11.5	050°	26.3°
3 Sept. j	1157	20°39.5′	156°46.6′	.72	.45	050°	26.51°
3 Sept. q	1330	20°39.5′	156°46.6′	8.58	7.11	120°	26.49°
3 Sept. t	1357	20°39.5′	156°46.6′	.89	.54	180°	26.51°
4 Sept. e	1126	20°40.2′	156°40.3′	1.79	.49	045°	25.90°
4 Sept. k	1158	20°39.0′	156°40.0′	3.93	3.58	100°	26.10°
4 Sept. n	1257	20°39.5′	156°36.9′	8.00	6.62	100°	26.20°
4 Sept. r	1324	20°40.0′	156°39.3′	6.30	5.27	111°	26.20°
4 Sept. v	1327	20°40.0′	156°39.3′	6.44	5.4	111°	26.20°
4 Sept. y	1353	20°39.5′	156°36.9′	4.92	4.07	110°	26.20°
5 Sept. b	1058	20°40.5′	156°35.7′	1.83	1.43	280°	26.6°
5 Sept. g	1124	20°40.1′	156°35.4′	1.39	.58	280°	26.7°
5 Sept. j	1354	20°46.8′	156°40.3′	3.35	2.99	225°	27.09°
6 Sept. c	1048	20°58.5′	156°45.3′	10.8	9.12	045°	25.95°
6 Sept. k	1124	20°58.0′	156°44.5′	10.2	8.85	045°	25.99°
6 Sept. q	1237	20°57.5′	156°44.0′	11.7	9.92	045°	26.3°
10 Sept k	1328	20°40.0′	156°38.3′	8.45	7.24	130°	26.60°
10 Sept. m	1333	20°40.0′	156°38.3′	7.15	6.00	130°	26.60°
10 Sept. r	1347	20°39.7′	156°39.3′	5.32	4.47	120°	26.59°
11 Sept. e	1317	20°45.5′	156°41.8′	5.45	3.75	210°	27.2°
11 Sept. f	1317	20°45.5′	156°41.8′	5.45	3.75	210°	27.2°
13 Sept. e	1308	20°17.6′	156°02.4′	2.41	1.97	090°	27.35°
13 Sept. f	1308	20°17.6′	156°02.4′	2.41	1.97	090°	27.35°
17 Sept. e	1136	20°29.9′	156°24.8′	9.79	8.31	086°†††	26.80°
17 Sept. c, h, k, n, q # #	{1111 / 1205}	20°28′	156°24′	9.74	8.18	088°†††	26.80°
17 Sept. A	1424	20°17.6′	156°14.8′	10.5	8.45	068°†††	26.90°

* Includes date of observation, 1951.
† Time meridian 150° W.
# Elevation above sea level.
# # Probability distribution derived from 5 photographic sets.

Values of the rms slope components σ_c, σ_u are given in Table I together with other pertinent data. The values will be different under different wind conditions, and in general they will depend on whether the sea surface is, or is not, covered by oil.

Equation (3) can be interpreted geometrically as follows. Let the two horizontal axes designate z_x, z_y and let the vertical axis designate the value of $p(z_x, z_y)$. The bell-shaped surface $p(z_x, z_y)$ is high near the coordinate center (representing the high probability of small slope) and falls off in all directions. The total volume under the curve is unity. In the case of high winds this volume is low and wide; for low winds it is high and narrow. The volume of a prism centered at z_x, z_y

TABLE I

Temp. (°C) Air at 2m	*Humidity (%)*	*Significant waves*			*Sea Surface*	*χ +Sun Az* **	*Mean Square Slope Components*	
		Ht (ft)	*Period (sec)*	*Direction (true)*			σ_c^2	σ_u^2
28.0°	69	3.5	4		clean	063°	.0211	.0390
27.75	69	6	5	056°	clean	057°	.0294	.0484
27.5°	65	6	5	056°	clean	036°	.0287	.0452
27.5°	65	6	5	056°	clean	047°	.0276	.0404
29.0°	58	1.5	3	059°	clean	095°	.00337	.00489
28.75°	61	2	3	101°	clean	140°	.0224	.0230
29.0°	58	—	—	—	clean	***	.0152	.0153
27.2°	69	1	2	120°	Nat. slick	120°	.00096	.00126
27.9°	67	1	2	100°	clean	94°	.00694	.00977
28.0°	69	2	3	106°	clean	126°	.0136	.0191
28.0°	67	4	3	106°	clean	136°	.0134	.0170
28.0°	67	4	3	106°	clean	119°	.0136	.0186
28.0°	69	4	3	100°	clean	***	.0172	.0174
27.0°	68	3	4	160°	clean	296°	.00534	.00906
27.1°	67	3	4	104°	clean	280°	.00609	.00875
27.0°	65	5	4	140°	clean	237°	.0102	.0125
27.2°	69	4	4	045°	clean	***	.0252	.0265
					oil slick	***	.0111	.0108
27.2°	71	4	4	045°	clean	040°	.0254	.0357
27.2°	69	5	4	045°	clean	045°	.0254	.0374
26.8°	81	3	3	090°	oil slick		.0102	.0117
26.8°	81	3	3	090°	oil slick	***	.00860	.0100
27.2°	76	3	3	090°	clean	***	.0137	.0179
					oil slick		.00967	.00985
27.3°	71	2	3	120°	clean	***	.0136	.0137
27.3°	71	2	3	120°	oil slick	***	.0107	.0109
28.4°	60	4	5	075°	oil slick	***	.00391	.00467
28.4°	60	4	5	075°	oil slick	076°	.00724	.00959
27.8°	76	4	3	080°	clean	080°	.0209	.0264
					oil slick		.0106	.0126
27.7°	77	4	3	080°	clean	087°	.0230	.0322
27.8°	79	5	3	080°	clean	069°	.0224	.0365

** True Azimuth of principal (y') axis.

*** Observed wind direction used.

††† Wind direction estimated from direction of wind streaks on water; recorded wind direction appears to be in error by twice magnetic variation.

with a base area $\delta z_x \delta z_y$ is the probability $p(z_x,z_y)\delta z_x \delta z_y$ for the occurrence of slopes within $z_x \pm \frac{1}{2}\delta z_x$, $z_y \pm \frac{1}{2}\delta z_y$.

Now take sections along various directions through the coordinate center. Each of these is nearly Gaussian and can be closely fitted by a Gaussian curve of equal standard deviation. Two of these sections (the principal sections) are of particular interest (Fig. 3): for one the equivalent Gaussian curve has greater standard deviation than any other section; the reverse is true for the other. These correspond to the direction of the smallest and largest mean square slope. Our observations show that they are oriented crosswind and up/downwind.

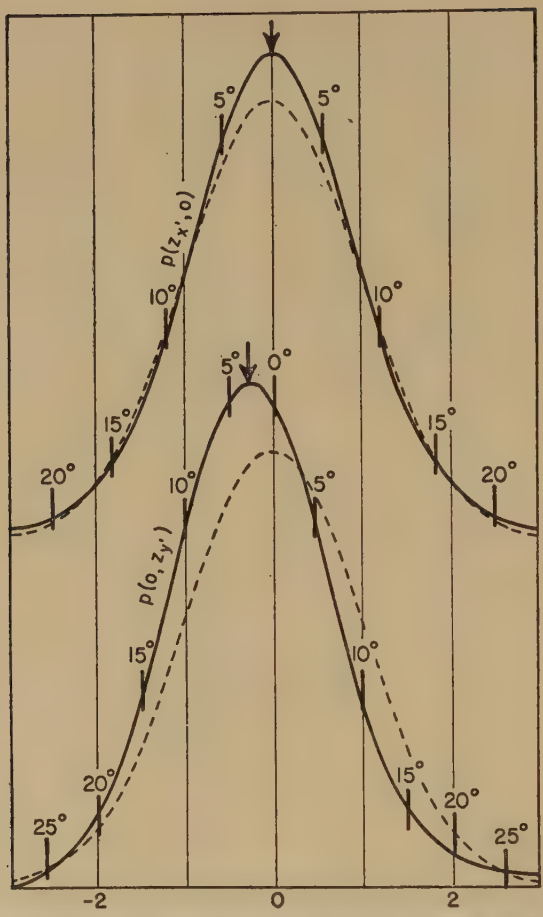

Figure 3. Principal sections through the probability distribution surface $p(z_x,z_y)$. The upper curves are along the crosswind axis z_x, the lower ones along the up/downwind axis z_y (positive upwind). The solid curves refer to the observed distribution, the dashed to a Gaussian distribution of equal mean square slope components. The thin vertical lines show the scale for both standardized slope components $\xi = z_x/\sigma_c$ and $\eta = z_y/\sigma_u$. The two scales for tilt, β, refer to a wind speed of 10 m sec^{-1}; skewness shown in the lower curve is computed for this wind speed. The modes are marked by arrows.

Another observed feature illustrated in Fig. 3 is an up- and downwind skewness. As a result, the most probable tilt is a few degrees, not zero, with the azimuth of ascent pointing downwind. Conversely, large slopes are more probable with azimuth of ascent pointed upwind. The skewness, as contained in the coefficients c_{21}, c_{03}, increases with increasing wind speed from nearly zero at very low winds to

$$c_{21} = -.11 \pm .03, \qquad c_{03} = -.42 \pm .12$$

at 14 m sec^{-1}.

The peakedness coefficients c_{40}, c_{22}, c_{04} are such as to make the very large and very small slopes more probable than those required for a Gaussian distribution (Fig. 3). The peakedness may be the result of variability in wind speed, but it is possible that systematic errors in the correction for background light may account for much of the observed peakedness. The peakedness coefficients show no significant variation with wind speed. The mean values are $c_{40} = .4 \pm .2$, $c_{22} = .1 \pm .05$, $c_{04} = .2 \pm .4$.

Oil slicks which cover an area of roughly one-fourth square mile reduce the mean square slope (regardless of direction) by a factor of two or three and eliminate skewness but leave peakedness unchanged.

There have been two other investigations of surface slopes. Duntley (1950) measured the surface slope components on Lake Winnipesaukee, N. H., by recording electrically the difference in immersion of pairs of thin vertical wires passing through the water surface. The wires were oriented to give simultaneous measurements of up/downwind and crosswind components. The separation between the wires on different occasions was 25 mm and 9 mm; consequently the measurements refer to the average value of slope over these distances. Schooley's (1954) observations from a bridge over the Anacostia River consisted of measuring the highlighted area on *resolved* photographs of the reflection of an artificial light source over the river. The results of their investigations agree in some points with ours, but there are significant discrepancies. Schooley's values of the mean square slopes are significantly *smaller* than ours for both high and low winds but agree at moderate wind speeds, whereas Duntley's values are 2.5 times *larger*. A discussion of these results has been given by Cox and Munk (1953).

4. SOME USEFUL RELATIONSHIPS

Of the many possible ways of describing the complexity of the sea surface, three in particular have been useful in modern work. Let f be some pertinent parameter with zero mean value such as elevation, slope, curvature, etc., and let $<f^2>$ be the mean square value (or variance) of f. According to the first approach, we let $\mathbf{T}_\omega \delta\omega$ be the contribution to $<f^2>$ by waves in the narrow, but not infinitely narrow (see Section 4.1), frequency band $\omega \pm \frac{1}{2}\delta\omega$. We can measure this quantity by recording it through an appropriate band pass filter, squaring the output, and averaging. It follows that

$$<f^2> = \int_0^\infty \mathbf{T}_\omega d\omega \tag{4}$$

is the mean square slope due to all frequencies. Here $\mathbf{T}_\omega$ is called the "frequency spectrum of the variance of f," or simply the spectrum.[2]

The second approach is the one we have taken. Let $p(f)df$ be the probability of slopes in the range $f \pm \frac{1}{2}df$. Then by definition

$$<f^2> = \int_0^\infty f^2 p(f) df. \tag{5}$$

Finally, a useful concept is the correlation (or mean displaced product)

$$\psi(a,b,\tau) = <f(x,y,t)f(x + a, y + b, t + \tau)> \tag{6}$$

between the value of f at position x,y and time t, and at $x + a$, $y + b$, and $t + \tau$. It is presumed that the surface is statistically uniform over time and space and that the corresponding averages are equal. For the special case $a = b = 0$, it can be shown (for example, see Rice, 1944: section 2) that the "auto correlation" is related to $\mathbf{T}$ according to

$$\psi(0,0,\tau) = \int_0^\infty \mathbf{T}_\omega \cos(\omega\tau) d\omega. \tag{7}$$

The foregoing equations show that the spectrum, the probability distribution, and the correlation are not unrelated. Our measurements of the probability distribution, therefore, have some bearing on the spectral representation of ocean waves. The required relationships, to be discussed (and made plausible, we hope) in this section, will be applied in the next.

[2] For the special case where f denotes the elevation z above mean sea level, the terms "energy spectrum" and "power spectrum" have been used. Strictly speaking, the energy spectrum is $\rho g \mathbf{T}_\omega$, as $\rho g \mathbf{T}_\omega(\omega)\delta\omega$ is the energy contained in the band $\omega \pm \frac{1}{2}\delta\omega$. The term power spectrum was originally introduced in electrical problems where it is convenient to measure the energy spectrum by recording the power dissipated in a unit resistance. But it is not suitable to oceanographic problems. An appropriate definition would be $\rho g \mathbf{v} \mathbf{S}$, where $\mathbf{v}(\omega)$ is the group velocity vector and $\mathbf{S}$ the directional spectrum of z^2 (Section 4.2). Then $\rho g \mathbf{v} \mathbf{S}(\omega, \alpha)\delta\omega\delta\alpha$ is the flux of energy in the frequency band $\omega \pm \frac{1}{2}\delta\omega$ into the direction $\alpha \pm \frac{1}{2}\delta\alpha$. This important spectrum, after integration over all frequencies, gives the angular distribution around a cylindrical island of the dissipation of energy. In deep water the magnitude of $\mathbf{v}$ is proportional to wave period, and the true power spectrum is therefore weighted in favor of the low frequencies relative to the energy spectrum.

4.1 *The frequency spectrum of the variance of elevations.* Most observations of ocean waves have been made at a single point in space, say the point $x = y = 0$. The result has been a record of $z(0,t)$ for a limited time, $2T$. Such a record may be represented in two ways. Since we have no information concerning the sea surface before or after the record, we may assume (A) that it repeats itself indefinitely over successive intervals, $2T$, or (B) that it is zero before and after the record. These assumptions lead to (A) Fourier series with periods $(2T)$, $\frac{1}{2}(2T)$, $\frac{1}{3}(2T)$, $\cdots$, or (B) Fourier integrals with all possible periods. It can be shown that the two representations are exactly the same for those periods contained in the series. For our purpose it is more convenient to use the second approach. Hence

$$z(0,t) = \int_{-\infty}^{\infty} g(\omega)e^{i\omega t}d\omega, \tag{8}$$

where

$$g(\omega) = (2\pi)^{-1}\int_{-T}^{T} z(0,t)e^{-i\omega t}dt \tag{9}$$

is the (complex) amplitude of a wave train of frequency ω.

But $g(\omega)$ is not a convenient function. It is sensitive to phase and its absolute value tends to increase as the length of record $2T$ increases. On the other hand, $|g(\omega)|^2 = g(\omega)g^*(\omega)$ is not phase-sensitive. Furthermore, it is readily measured by passing the wave-generated signal through a narrow tuned filter. Since by hypothesis the sea surface is statistically uniform in time, the mean square of the sea surface elevation must exist. According to Parseval's theorem (Titchmarsh, 1937)

$$\langle z^2(0,t)\rangle = \lim_{T\to\infty}\frac{1}{2T}\int_{-T}^{T} z^2(0,t)dt$$

$$= \lim_{T\to\infty} 2\pi\int_{-\infty}^{\infty}\frac{g(\omega)g(-\omega)}{2T}d\omega = \lim_{T\to\infty} 4\pi\int_{0}^{\infty}\frac{|g|^2}{2T}d\omega. \tag{10}$$

The last equality follows because z is a real quantity, hence from (9) $g(-\omega) = g^*(\omega)$.

The existence of the limit of the integral in (10) does not necessarily imply the existence of the limit of the integrand. It is tempting to assume that it does, for then the limit of $4\pi|g|^2/2T$ as $T \to \infty$ equals the spectrum $\mathbf{T}_\omega$ in accordance with (4). Surprisingly, this is not the case for waves which result from a large number of impulses randomly

applied to the sea surface. A plot of $|\bar{g}|^2/2T$ against ω is then a wiggly line which oscillates more and more wildly as the record length is increased. The difficulty can be removed by defining $\bar{g}^2$ as a smoothed version of $|g|^2$ averaged over an arbitrarily small but *finite* range. The limit

$$\mathbf{T}_\omega = \lim_{T\to\infty} \frac{4\pi\bar{g}^2}{2T} \tag{11}$$

then exists, and equation (10) can be written

$$<z^2> = \int_0^\infty \mathbf{T}_\omega d\omega. \tag{12}$$

A rigorous mathematical approach[3] uses a Lebesgue integral formula in place of (10).

4.2 *The directional spectrum of the variance of elevation.* In contrast to measurements at a fixed point, the slope distribution was measured at a single instant. We may connect these two types of measurements by means of the wave equation. Suppose that z and $\partial z/\partial t$ are specified at $t = 0$ within the area $-S < x < S$, $-S < y < S$. Then

$$z(x,y,t) = \mathrm{Re} \int_{-\infty}^{\infty}\int_{-\infty}^{\infty} A(k_x,k_y) \exp i(k_x x + k_y y - \omega t) dk_x dk_y \tag{13}$$

satisfies the specified initial conditions, provided (Longuet-Higgins, 1950)

$$A(k_x,k_y) = \frac{1}{2\pi}\int_{-S}^{S}\int_{-S}^{S}\left(z - \frac{1}{i}\frac{\partial z}{\partial t}\right)_{t=0} \exp - i(k_x x + k_y y) dx dy. \tag{14}$$

Equation (13) represents z as a series of elementary wave trains of wave length $2\pi/k$, where $k^2 = k_x^2 + k_y^2$, frequency $\omega(k)$, phase velocity $C = \omega/k$ in the direction of the vector (k_x,k_y), and amplitude $A(k_x,k_y)\, dk_x dk_y$. Each elementary train obeys the wave equation $\nabla^2 z = C^{-2}\partial^2 z/\partial t^2$. The sea surface has been assumed flat at $t = 0$ for $|x| > S$, $|y| > S$, and because of this assumption the forecasting value of (13) will deteriorate with time. This difficulty can be avoided by increasing the area $4S^2$ without limit. In particular, it can be shown (Cox and Munk, 1953) that if

$$\mathbf{S} = \lim_{S\to\infty} \frac{2\pi^2\bar{A}^2}{4S^2}, \tag{15}$$

[3] See, for example, Wiener (1933). The application of the Lebesgue integral to ocean wave analysis is largely due to Pierson and his collaborators (Pierson and Marks, 1952).

where $\overline{A}^2$ is a smoothed version of $|A|^2$ (analogous to the relation between $\bar{g}^2$ and $|g|^2$), then

$$\psi(a,b,\tau) = \int_{-\infty}^{\infty}\int_{-\infty}^{\infty} S\cos(k_x x + k_y y - \omega\tau)dk_x dk_y. \qquad (16)$$

The way is now open to find the connection between the frequency spectrum, $\mathbf{T}_\omega$, and the directional spectrum $\mathbf{S}$. Setting $a = b = 0$ and changing variables from (k_x,k_y) to (ω,α), we have

$$\psi(0,0,\tau) = \int_0^{\infty}\int_{-\pi}^{\pi}\mathbf{S}(\omega,\alpha)\left|\frac{\partial(k_x,k_y)}{\partial(\omega,\alpha)}\right|\cos(\omega\tau)d\alpha d\omega, \qquad (17)$$

where $\partial(k_x,k_y)\partial(\omega,\alpha)$ is the Jacobian of the transformation. A comparison with (7) leads to

$$\mathbf{T}_\omega = \int_{-\pi}^{\pi}\mathbf{S}(\omega,\alpha)\left|\frac{\partial(k_x,k_y)}{\partial(\omega,\alpha)}\right|d\alpha, \qquad (18)$$

which is the desired relation.

There are two approximations inherent in the stated form of the wave equation which limit the applicability of these results: (A) nonlinear terms have been neglected and (B) no allowance has been made for generation and decay of waves. The first error may be associated with the fact that the observed distribution of slopes showed a slight positive peakedness relative to a Gaussian distribution while the linear equation predicts a strictly Gaussian distribution for the statistically steady state. The second error will cause the predicted form of the sea surface to disagree with equation (13) for $t > 0$, but if the fetch and duration of the wind are large enough so that "equilibrium waves" are present, then the statistical behavior of the sea surface is sufficiently well represented. Since very short waves generate and decay most rapidly, the uncertainty of the results is greatest for large values of k and ω.

Note that the evaluation of the directional spectrum requires a knowledge of both z and $\partial z/\partial t$ at the initial time. Clearly the information $z(x,y,0)$ from a single snapshot could not tell us whether the waves are travelling in one direction or in the opposite one. Yet the topography shown on such a snapshot can be represented by a Fourier spectrum. We shall call this the *two-dimensional* spectrum. It differs from the *directional* spectrum inasmuch as it contains only directions in the range $-\frac{1}{2}\pi$ to $+\frac{1}{2}\pi$ as compared to $-\pi$ to $+\pi$. For any particular direction, α, the two-dimensional spectrum equals $\mathbf{S}(\alpha) + \mathbf{S}(\alpha+\pi)$. If the directional spectrum is narrow and contains only small contributions from directions outside $-\frac{1}{2}\pi < \alpha < +\frac{1}{2}\pi$,

then the two spectra are nearly the same with regard to the surface elevation. However, the slight difference may be of importance at great depths where wave trains travelling oppositely lead to oscillations which Longuet-Higgins (1950) suggests are a cause of microseisms.

4.3 *Slope spectra and mean square slopes.* The relation (16) between the correlation and the directional spectrum permits a comparison of spatial observations (such as the slope distribution as determined by glitter observations) with records obtained at a single point. The starting point is equation (6), with f designating the elevation z. The method is to differentiate (6) and (16) with respect to a,b to obtain [4]

$$-\frac{\partial^2\psi}{\partial a^2} = \langle z_x(x,y,t)z_x(x+a, y+b, t+\tau)\rangle$$

$$= \int_{-\infty}^{\infty}\int k_x^2\mathbf{S}\cos(k_x x + k_y y - \omega\tau)dk_x dk_y \qquad (19)$$

$$-\frac{\partial^2\psi}{\partial b^2} = \langle z_y(x,y,t)z_y(x+a, y+b, t+\tau)\rangle$$

$$= \int_{-\infty}^{\infty}\int k_y^2\mathbf{S}\cos(k_x x + k_y y - \omega\tau)dk_x dk_y.$$

Comparison with (16) shows that $k_x^2\mathbf{S}$ and $k_y^2\mathbf{S}$ are the spectra of the slope components, z_x and z_y. For the case $a = b = 0$, equation (18) reduces to

$$\langle z_x^2\rangle = \int_{-\infty}^{\infty}\int k_x^2\mathbf{S}dk_x dk_y, \qquad \langle z_y^2\rangle = \int_{-\infty}^{\infty}\int k_y^2\mathbf{S}dk_x dk_y. \qquad (20)$$

With the y-axis pointing upwind, these are the crosswind and up/downwind components of mean square slopes σ_c^2 and σ_u^2. On changing to the variables (k,α), one obtains finally

$$\sigma_c^2 = \int_0^{\infty}\int_{-\pi}^{\pi} k^2\sin^2\alpha\mathbf{S}kdkd\alpha, \qquad \sigma_u^2 = \int_0^{\infty}\int_{-\pi}^{\pi} k^2\cos^2\alpha\mathbf{S}kdkd\alpha \qquad (21)$$

and

$$\sigma^2 = \sigma_c^2 + \sigma_u^2 = \int_{-\infty}^{\infty}\int k^2\mathbf{S}dk_x dk_y = \int_0^{\infty} k^2\mathbf{T}_\omega d\omega. \qquad (22)$$

The last expression follows from (17) and (18).

[4] For example, see Eckart (1953): eq (37).

5. INTERPRETATION

The spectrum of the sea surface has been written in different ways by different authors. We now consider whether their mathematical models are consistent with our observations. First we seek to find the simplest model consistent with two observed features: the nearly Gaussian distribution of slopes (Section 5.1) and the appropriate ratio of up/downwind to crosswind mean square slope components (5.2). These features do not place any severe restrictions on the dependence of the slope spectrum on wave frequency. In Sections 5.3 and 5.4 the more complicated models proposed respectively by Darbyshire and Neumann are examined. Only the Neumann wave spectrum is consistent with the remaining principal features of the observed slope distribution: the linear increase of mean square slope with wind speed.

5.1 *Waves in one dimension.* The simplest model consists of a set of sinusoidal waves having one frequency and one direction. If such waves existed on the ocean surface they would have infinitely long crests. The slope distribution would be one-directional and the glitter pattern would consist of a single streak along some line α = constant. Clearly this is not in accord with the pattern shown on Figs. 1 and 2.

In addition to this discrepancy, the model leads also to frequency distributions of slopes which differ essentially from the observed distribution. The most probable slopes of a single sine wave are the slopes at the inflection points (say $\pm A$), where their values are stationary—and at a maximum. The probability $p(z_x)\delta z_x$ for slopes between $z_x \pm \frac{1}{2}\delta z_x$ is given by

$$\pi^{-1}(A^2 - z_x^2)^{-\frac{1}{2}} \tag{23}$$

for $z_x^2 < A^2$, and zero otherwise. The distribution is bimodal as shown in Fig. 4.

Next we consider the linear superposition of N sine waves

$$z_x = \sum_{j=1}^{N} A_j \cos(k_j x + \varphi_j). \tag{24}$$

We assume that the ratio of any two wave numbers, k_l/k_m, is irrational. The slope component is then an example of the "almost periodic function" of H. Bohr. As implied by its name, the almost periodic function comes close to being periodic but never quite repeats itself, a property which is in accord with our impressions of the real sea surface. The irrationality of the wave number forbids that equation (24) could represent any wave phenomenon in which the waves have rational "overtones," for example, Stokes waves of finite amplitude or seiches of a shallow rectangular body of water. In the open sea these are not believed to be serious limitations.

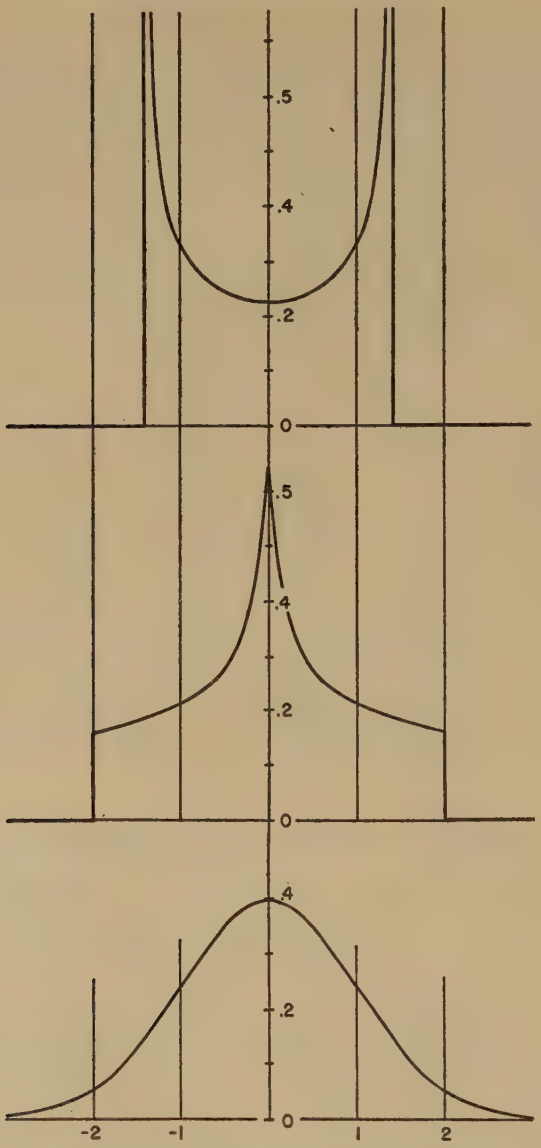

Figure 4. Top. Slope probabilities resulting from one sine wave. Middle. The linear superposition of two sine waves of equal maximum slope and irrational periods. Bottom. The linear superposition of an infinite number of irrational sine waves. The horizontal scale is $\xi = z_x/\sigma_x$; the vertical scale gives $p(z_x)$ in units of $1/\sigma_x$.

With the proviso of irrational wave numbers, the slope z_x due to any of the N components is uncorrelated with that of any other, and the calculation of the distribution of z_x is an example of the problem of random flights (for example, see Chandrasekhar, 1943). Cox and Munk (1953) found that

$$p(z_x) = \pi^{-1} \int_0^\infty \cos(\rho z_x) \left[\prod_{i=1}^{N} J_0(\rho A_i) \right] d\rho. \tag{25}$$

For the special case of a single wave number ($N = 1$), this reduces to (23); for *two* waves of equal amplitude A, this reduces to

$$\pi^{-2} A^{-1} K[1 - (z_x/2A)^2]^{-\frac{1}{2}} \tag{26}$$

for $z_x^2 < 4A^2$, and zero otherwise, where $K(x) = \int_0^{\frac{1}{2}\pi} (1 - x^2 \sin^2 t)^{-\frac{1}{2}} dt$ is the elliptic integral. In this case the distribution has a single logarithmically infinite maximum (Fig. 4). In the case of two unequal waves there would be two such maxima. For three sine waves there are no infinite peaks in the distribution function. In a general way it can be seen that the distribution approaches the Gaussian distribution as N increases. When N is large and when all N components are equal, equation (25) reduces to

$$(2\pi)^{-\frac{1}{2}} \sigma_x^{-1} e^{-\frac{1}{2}\xi^2} [1 - (\xi^4 - 6\xi^2 + 3)/(16N) + \cdots], \tag{27}$$

where σ_x^2 is the mean square slope and $\xi = z_x/\sigma_x$. This series is of the Gram-Charlier type, with the second term in the square bracket representing peakedness.[5] Comparison with equation (3) for the two-dimensional type reveals that the peakedness coefficient c_{40} is equivalent to $-(3/2N)$. Thus the foregoing expression leads to a negative peakedness, whereas the observed peakedness is positive. Hence the experimental results provide no evidence for discrete spectral components in the ocean waves.

A sea surface with a *continuous* spectrum of waves may be considered as the result of increasing the number N of discrete components without limit. In this case equation (27) reduces to a Gaussian distribution.

5.2 *"Beam width" of the trade wind sea.* In the preceding section we have learned that the observed distribution is consistent with a continuous spectrum in two dimensions. The next problem is to interpret the observed ratio σ_c^2/σ_u^2 in terms of the dependence of the directional spectrum **S** on the direction α. Clearly, if **S** were the same in all directions, then the crosswind and up/downwind slopes would

[5] A similar development can be found in Sȳno (1953).

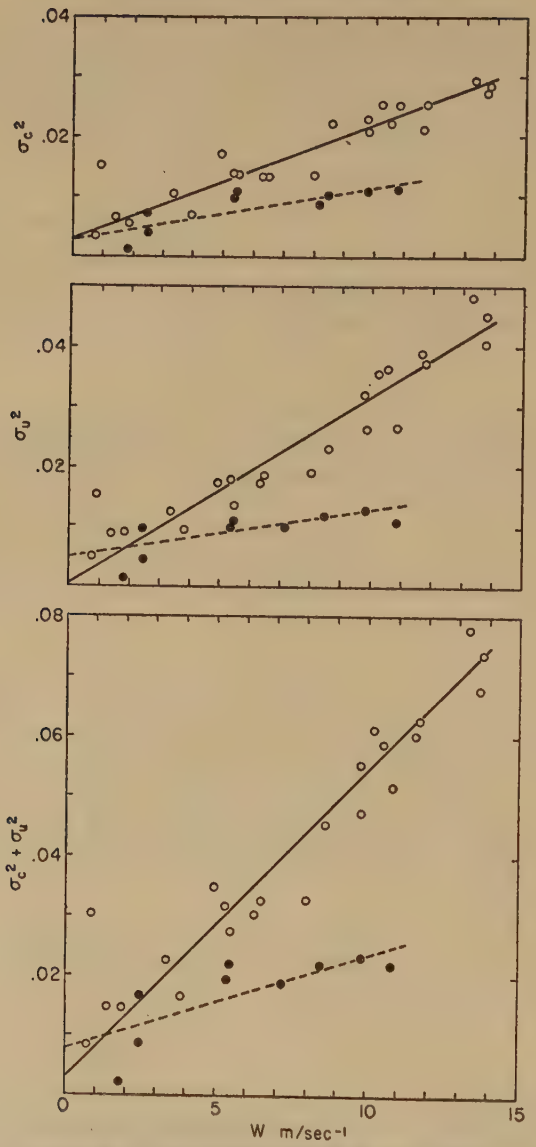

Figure 5. Mean square slope components and their sum as functions of the wind speed, W, measured 41 feet above sea level. The plot includes all analyzed data for clean sea surface (open circles) and slick surfaces (solid circles). Continuous lines are regression lines for clean surface; dashed lines for slick surface.

be equal and their ratio would be unity. On the other hand, if **S** were confined to a narrow range on both sides of the wind, then the cross-wind component would be very small compared to the up/downwind component of mean square slopes. The measured values (Fig. 5, Table I) lie between these extremes and indicate a broad but nonetheless directional "beam pattern." The large variability in the ratio σ_c^2/σ_u^2 (Table II) is far in excess of experimental error. It is probably the result of differences, from one case to the next, in the variability of the wind direction. Steady winds would lead to small values in σ_c^2/σ_u^2, whereas gusty winds would diminish this ratio to somewhere near unity.

According to equation (21),

$$\frac{\sigma_c^2}{\sigma_u^2} = \frac{\int_0^\infty \int_{-\pi}^{\pi} k^2 \sin^2 \alpha \, \mathbf{S}(k,\alpha) k dk d\alpha}{\int_0^\infty \int_{-\pi}^{\pi} k^2 \cos^2 \alpha \, \mathbf{S}(k,\alpha) k dk d\alpha}.$$

The simplest assumption we can make is that the directionality is the same for all wave numbers, k, and that the beam pattern is sharply bounded at $\alpha = \alpha_0$. Hence

$$\mathbf{S} = F(k) \quad \text{for} \quad -\alpha_0 < \alpha < \alpha_0,$$

and zero otherwise. This gives

$$\frac{\sigma_c^2}{\sigma_u^2} = \frac{2\alpha_0 - \sin 2\alpha_0}{2\alpha_0 + \sin 2\alpha_0}, \tag{28}$$

as shown in Fig. 6. For a narrow beam the above function reduces to $\frac{1}{3}\alpha_0^2$.

For two infinitely narrow cross beams intersecting at an angle $2\alpha_0$, we set

$$\mathbf{S} = F(k) \quad \text{for} \quad \alpha = -\alpha_0, \quad \alpha = +\alpha_0,$$

and zero otherwise. This yields simply

$$\sigma_c^2/\sigma_u^2 = \tan^2 \alpha_0. \tag{29}$$

TABLE II. Beam Widths and Angular Spread Between Two Intersecting Beams, Leading to Observed Ratios of Crosswind and Up/Downwind Slope Components

	Min.	*Mean*	*Max.*	*Slick (mean)*
σ_c^2/σ_u^2	0.54	0.75	1.0	0.86
$2\alpha_0$, single beam	134°	157°	180°	167°
$2\alpha_0$, two narrow cross beams	72°	82°	90°	86°

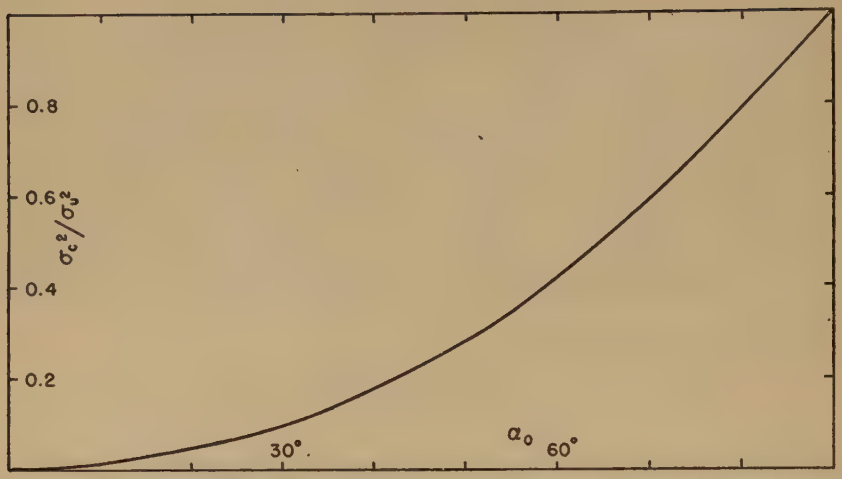

Figure 6. Half beam width of wave directions, α_0, as a function of the ratio of mean square slope components, σ_c^2/σ_u^2. It is assumed that waves of all periods have the same beam width.

The corresponding values are given in Table II. For a trade-wind sea, it is believed that the single broad beam conforms more nearly to actual conditions. The corresponding beam width is remarkably wide. For comparison, Duntley (1950) obtained $\sigma_c^2/\sigma_u^2 \approx 0.7$ on Lake Winnipesaukee, N. H.; Schooley (1954) obtained a smaller value, about 0.4, possibly because his photographs from a bridge over the Anacostia River sampled a relatively small area with a correspondingly smaller variability in wind direction. It should be kept in mind, however, that all of these values refer to those (high frequency) components of the spectrum that contribute largely to slopes. There are no other published measurements of the directionality of ocean waves, but preliminary results obtained by Barber (personal communication) by means of an array of wave *height* recorders indicate a beam width of 90°. This agrees exactly with Arthur's (1949) estimate based on a comparison between observed and predicted waves during the invasion of Sicily. However, it is becoming clear that the beam width varies considerably with meteorological conditions, so that a great deal of further work remains to be done.

5.3 *The spectra proposed by Darbyshire and Neumann.* The period spectrum[6] $\mathbf{T}_T$ is related to the frequency spectrum $\mathbf{T}_\omega$ by the relation

[6] A choice of notation must be made between the use of frequencies and wave numbers on the one hand or of periods and wave lengths on the other hand. The physicist is more familiar with the former notation, the oceanographer with the latter.

$$\mathbf{T}_\omega |d\omega| = \mathbf{T}_T |dT|, \tag{30}$$

where $\omega = 2\pi/T$, $k = 2\pi/L$, and

$$\omega^2 = gk + \gamma k^3, \tag{31}$$

with γ designating surface tension divided by density (74 cm^3 sec^{-2} for clean water). According to (31), the phase velocity reaches a minimum value

$$C_{min} = \omega_m/k_m = (4g\gamma)^{1/4} \tag{32}$$

when

$$\omega_m = (4g^3/\gamma)^{1/4}, \qquad k_m = (g/\gamma)^{1/2}.$$

Numerical values are $C_{min} = 23$ cm sec^{-1}, $T_m = 0.074$ sec, $L_m = 1.7$ cm.

Waves much longer than L_m are gravity waves, and for these

$$\omega^2 \approx gk. \tag{32}$$

Waves much shorter are capillary waves, and

$$\omega^2 \approx \gamma k^3. \tag{33}$$

Darbyshire (1952) has proposed a spectrum of the variance of $z(0,t)$ equivalent to

$$\mathbf{T}_T = c'T^2 \exp\left[-2.0\left(\frac{gT}{U} - 4.6\right)^2\right], \tag{34}$$

where c' has the value 22 $cm^2 sec^{-3}$ and U is the gradient wind speed equal on the average to 1.5 times the masthead wind speed, W.

The spectrum was obtained by frequency-analysis of pressure records of waves generated by local storms at Lands End, England. Only those storm records were analyzed for which the fetch was sufficient to generate equilibrium waves. The bottom pressure transducer was usually located at a depth of 50 ft. This requires that for wave periods less than 14 sec the usual hydrodynamic relationship must be used to convert bottom pressure to surface elevation, as has been done by Darbyshire. But for periods less than 6 sec, the bottom pressure oscillations are reduced to such a low level that this is no longer

---

Most relationships are somewhat simpler in the former notation, but the integrals appearing in this section must actually be converted to the latter notation to be put into integrable form. We have made the following compromise. In sections dealing with the theory of spectra we have used the former notation. But in the following sections, where we are mostly concerned with numerical values of waves whose periods greatly exceed 1 second and whose lengths exceed 1 cm, it seemed preferable to adopt the latter convention.

practicable. Apparently these short-period waves have been ignored by Darbyshire. But it will be shown that these waves contribute about five-sixths of the total wave energy and that consequently Darbyshire's spectrum is too narrow and the total energy too small (Fig. 7). A pressure recorder at 50 ft is evidently not a suitable instrument for obtaining the energy spectrum.

On the basis of visual observations of fully developed waves in a storm area, Neumann (1953) proposed a spectrum (Fig. 5)

$$\mathbf{T}_T = \frac{1}{8} c \left(\frac{gT^2}{2\pi}\right)^2 \exp\left[-2\left(\frac{gT}{2\pi W}\right)^2\right], \tag{35}$$

where W is the wind speed and

$$c = 0.827 \times 10^{-3}\ \text{sec}^{-1}. \tag{36}$$

It is of interest to compare the Darbyshire and Neumann spectra. The periods which correspond to the maximum value of $\mathbf{T}_T$,

$$4.7\, g^{-1}U \approx 7.1\, g^{-1}W, \qquad 2\pi g^{-1}W \tag{37}$$

respectively, are in reasonable agreement. The mean square elevations,[7] however, follow different laws:

$$6.4 \times 10^{-5}\ \text{cm}^{-1}\ \text{sec}^3\ U^3, \qquad 3.2 \times 10^{-12}\ \text{cm}^{-3}\ \text{sec}^5\ W^5. \tag{38}$$

If the observations in Darbyshire's fig. 7 are fitted to Neumann's formula and if $<z^2>$ is computed as a function of W, we find that $c = 0.3 \times 10^{-3}\ \text{sec}^{-1}$ compared to Neumann's value 0.8×10^{-3}. The small value presumably reflects the lack of information on wave periods less than $T_1 = 6$ sec. We propose to correct this value as follows. Assume Neumann's spectrum (35). The contribution of waves having periods greater than T_1 to the mean square elevation is

$$<z^2>_{T>T_1} = \int_{T_1}^{\infty} \mathbf{T}_T dT = \left(\frac{g}{2\pi}\right)^2 \frac{c}{8} \left\{\frac{1}{2} T_1^3 V^2 \left(1 + \frac{3}{2}\frac{V^2}{T_1^2}\right) e^{-T_1^2/V^2} + \frac{3}{8} V^5 \sqrt{\pi}\left[1 - H\left(\frac{T_1}{V}\right)\right]\right\}, \tag{39}$$

[7] The average kinetic and average potential energy for gravity waves equal $\frac{1}{2}\rho g <z^2>$. The potential energy due to surface tension may be estimated as follows. The increase of surface area due to waves is $\int\int_A (\sec\beta - 1)dxdy$ and the potential energy per unit area is $(g\gamma/A)\int\int(\sec\beta - 1)dxdy \approx g\gamma\sigma^2/2$. The potential energy increases linearly with σ^2, hence it is proportional to wind speed and reaches a value of 2.8 erg cm^{-2} at $W = 14\ m\ \text{sec}^{-1}$. According to the Neumann energy spectrum, this is 3×10^{-7} times the potential energy due to gravity waves under similar conditions.

where $V = \pi\sqrt{2}\, Wg^{-1}$ and $H(\xi) = 2\pi^{\frac{1}{2}} \int_0^{\xi} e^{-t^2}\, dt$ is the error integral.

Entering equation (39) with appropriate values of W and $<z^2>_{T>T_1}$ from Darbyshire's data and setting $T_1 = 6$ seconds, we obtain $c = 2 \times 10^{-3}$ sec^{-1} with large scatter compared to the previous value of 0.3×10^{-3} sec^{-1} (uncorrected for the high frequency cut-off) and Neumann's value 0.8×10^{-3} sec^{-1}.

5.4 *The slope spectrum and mean square slope.* The mean square slope, regardless of direction, σ^2, can be computed from $\mathbf{T}_T$ according to equations (22) and (30). *Neglecting capillary waves*, the spectra proposed by Darbyshire and Neumann yield, respectively,

$$(2\pi)^4 \sqrt{\left(\frac{1}{2}\pi\right)} (4.6)^{-2} c'(gU)^{-1} = 1.0\, W^{-1} \tag{40}$$

$$\frac{1}{2}\pi^3 \sqrt{\left(\frac{1}{2}\pi\right)} cg^{-1}W = 1.6 \times 10^{-5} W. \tag{41}$$

By the method of least squares, our observations give

$$\begin{aligned} &5.12 \times 10^{-5} W + 0.003 \pm 0.004 \\ &1.56 \times 10^{-5} W + 0.008 \pm 0.004 \end{aligned} \tag{42}$$

for the clean and slick surface, respectively. Here W is in cm sec^{-1}.

Contrary to our observations, the Darbyshire spectrum predicts that the mean square slope *decreases* with increasing wind speed. For $W = 10$ m sec^{-1}, $\sigma^2 = 10^{-3}$ compared to the observed value $(54 \pm 4) \times 10^{-3}$. Clearly the spectrum proposed by Darbyshire has too little energy in the short waves. As noted earlier, this is not surprising, since waves having periods shorter than six seconds could not have been observed.

The important result is that Neumann's spectrum yields the observed linear relation between mean square slope and wind speed.[8] Furthermore, the computed proportionality constant agrees with the measurements over slicks, but it is one third the value required to account for the clean surface. If we take the value $c = 2 \times 10^{-3}$ sec^{-1} on the basis of Darbyshire's data (corrected for high frequency cut-off), the result is

$$\sigma^2 = 4 \times 10^{-5} W.$$

[8] This fact was mentioned by W. Pierson in a paper delivered before the American Geophysical Union, May 1953.

A generalization of Neumann's spectrum of the form

$$\mathbf{T}_T \sim T^m \exp\,[-\,(T/W)^n]$$

yields

$$\sigma^2 \sim W^{m-3}\,\frac{1}{n}\,\Gamma\left(\frac{m-3}{n}\right),$$

and hence σ^2 will be proportional to W only if $m = 4$, as assumed by Neumann. Neumann states that his data are convincingly better in accord with $\mathbf{T}_T \sim T^4$ than T^3 or T^5. Of course there must be other analytic functions which also yield $\sigma^2 \sim W$. Nevertheless the consistency of Neumann's result with ours is encouraging.

Next we wish to examine whether or not an exact integration which considers capillaries leads to a measurable deviation from the linear relation between σ^2 and W. We assume without justification that Neumann's spectrum function can be extended into the high frequencies. The modification is such that for $T \ll T_m$ the slope spectrum decreases with decreasing T like $T^{8/3}$ instead of remaining constant (Fig. 7), so that the mean square slope must be less than that given by (41). It is no longer possible to obtain an integral in closed form. We derived analytic solutions for the two asymptotic cases, $W \ll c_{\min}$ and $W \gg c_{\min}$, and integrated the intermediary part by numerical methods. The resultant mean square slope is

$$\sigma^2[1 - 2.28\pi^{-\frac{1}{3}}\,(c_{\min}/W)] = \sigma^2 - 0.0005, \qquad (43)$$

where σ^2 is the solution (eq. 41) when capillarity is neglected. The measured intercept (eq. 42) is $+\,0.003 \pm 0.004$. The modification is evidently smaller than the uncertainty in the empirical relations.

6. THE EFFECT OF SLICKS

We wish to consider whether it is possible to account for the observed reduction by a factor of two or three of the mean square slopes. The method will in a sense be the opposite of that in Section 4.2. There we assumed a statistical balance between generation and decay. Here we propose no generation and full decay by molecular viscosity.

According to Reynolds's classical theory (Lamb, 1932: 631–632), an inextensible surface film in effect annuls the horizontal velocity at the surface. This leads to a modulus of decay of

$$\tau = 2\sqrt{2}\,\nu^{-\frac{1}{2}} k^{-1} \omega^{-\frac{1}{2}},$$

where ν is the kinematic viscosity. In the actual case, the film will be somewhat extensible, and the foregoing expression may be regarded as an upper limit to the effectiveness of a surface active agent. The re-

duction in (amplitude)^2 for each spectral component is exp $(-2t/\tau)$, where t is the length of time since the wave entered the slick. The time required to cross a slick of length S is $t' = Sk/\omega$, and the mean reduction (sampled by a photograph of the entire slick) is

$$F = \frac{1}{t'} \int_0^{t'} e^{-2t/\tau}\, dt = \alpha(1 - e^{-1/\alpha}),$$

where

$$\alpha = (2\omega)^{\frac{1}{2}} S^{-1} \nu^{-\frac{1}{2}} k^{-2} = 2.11 \times 10^{-4} k^{-2} \omega^{\frac{1}{2}} cgs$$

for a slick 500 m in length. For $\alpha \gg 1$, $F \approx 1$, and for $\alpha \ll 1$, $F \approx \alpha$. The two above equations with $\omega(k)$ lead to $F(T)$. This reduction factor has been applied to the (amplitude)^2 and (slope)^2 spectra, as shown in Fig. 7. For waves of 0.5 sec (1 ft length), these spectra are reduced by a factor of 100 (amplitude by a factor of 10), and thus waves shorter than this are essentially eliminated. This is in reasonable accord with visual observations. As is to be expected, the mean square amplitude is hardly affected by this "high frequency cut-off," whereas the mean square slope is appreciably reduced.

The mean square slope in the presence of slicks, $\int_0^\infty Fk^2\, \mathbf{T}_T\, dT$, equals

$$0.34 \times 10^{-2}, \qquad 0.76 \times 10^{-2}$$

for wind speeds of 5 m sec^{-1} and 10 m sec^{-1} respectively. The corresponding ratios in mean square slope with slick as compared to those with a clean surface are

$$0.40/0.82 = 0.48, \qquad 1.13/1.65 = 0.68.$$

The observations give

$$0.55, \qquad 0.44.$$

The numerical values show rough agreement between the observed decrease in mean square slope within the slick and that computed on the basis of Reynolds' classical theory. But some serious difficulties remain. Reynolds' theory presumes a (horizontally) inextensible surface film such as one would expect to find for a monomolecular layer or for layers a few molecules thick at most. On the other hand, the thickness of the artificial slicks is estimated to be of the order of 10^{-4} cm, or 1000 molecules. This estimate follows from considerations involving the known size of the slick and of the volume of oil and from the occasional appearance of interference colors.

It is possible, however, that the oil film had an adsorbed monolayer at the air-oil or oil-water interface.[9] The compressional strength of

[9] See also Hennicker (1949). He summarizes experimental evidence for crystal-like organization of polymolecular films. Such a film would be expected to withstand static forces.

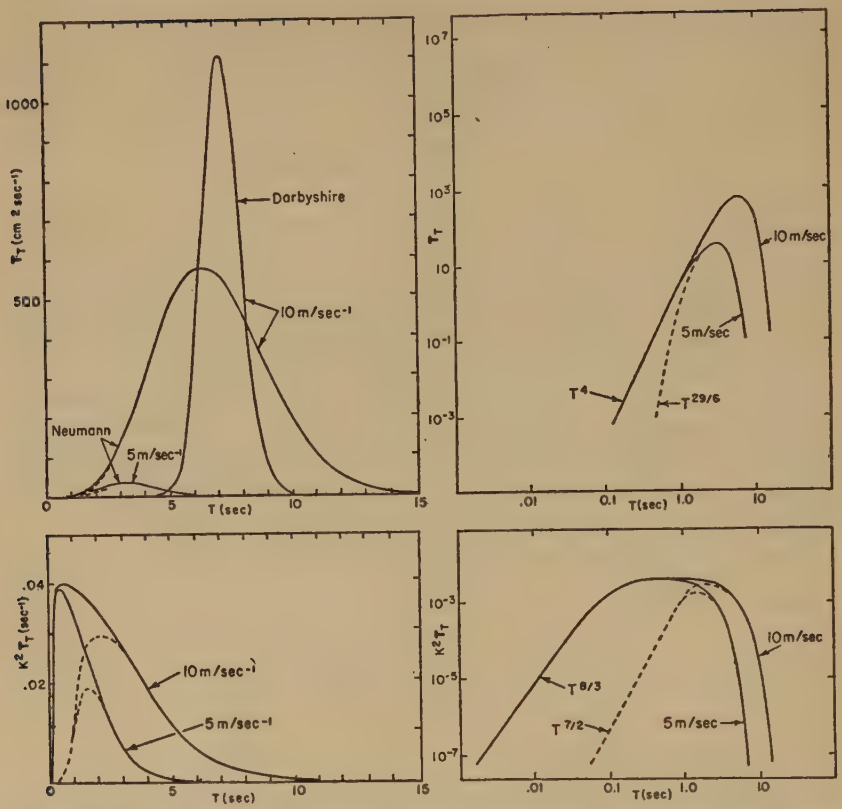

Figure 7. Period spectra of variance of sea surface elevation (upper panels) and of slope regardless of direction (lower panels). The left panels are drawn on a linear scale, the right panels on a double logarithmic scale. The asymptotic behaviour for high frequencies is indicated. Curves refer to wind speeds of 5 and 10 m sec^{-1} as noted. Solid lines apply to clean sea surface, dashed lines to slick surface. The variance of the $z(t)$ spectrum proposed by Darbyshire is illustrated on the upper left panel; all other curves are derived from Neumann's spectrum.

such a layer would be the difference between the surface tension of a clean interface ($\approx$ 40 dynes cm^{-1} for oil-water) and the surface tension of the contaminated surface ($>$ 0 dynes cm^{-1}). The following calculation shows that this would not be sufficient to annul the surface orbital velocities.

The x,y components of stress induced in the film by horizontal shear in the orbital velocity just below the film are

$$p_{xz} = \mu\left(\frac{\partial w}{\partial x} + \frac{\partial u}{\partial z}\right), \qquad p_{yz} = \mu\left(\frac{\partial w}{\partial y} + \frac{\partial v}{\partial z}\right),$$

where u,v,w are the x,y,z components of orbital velocity of the waves, μ is the viscosity, and the derivatives are to be evaluated at the surface. Let $\mathbf{p}$ be the vector shear whose components are p_{xz} and p_{yz}. For an infinitesimal wave train in the direction $\mathbf{k}$ (unit vector $\mathbf{k}_1$) of elevation

$$Re\,\{A\,\exp\,[i(kr - \omega t)]\}kdkd\alpha,$$

the appropriate formula is (Lamb: Arts. 349, 351)

$$\mathbf{p} = \mathbf{k}_1\omega^{3/2}(\rho\mu)^{\frac{1}{2}}\,Re\,\left\{A\,\exp\left[i\left(\mathbf{k}\cdot\mathbf{r} - \omega t - \frac{\pi}{4}\right)\right]\right\}kdkd\alpha.$$

Consider two points, $\mathbf{r}_1$ and $\mathbf{r}_2$, and let $\Delta\mathbf{r} = \mathbf{r}_2 - \mathbf{r}_1$. Then, if there is no shear strength in the film, the scalar

$$F_{12} = \int_{\mathbf{r}_1}^{\mathbf{r}_2} \mathbf{p}\cdot d\mathbf{r}$$

is the *difference* in tension between the two points. For the wave train, this gives

$$F_{12} = 2\omega^{3/2}(\rho\mu)^{\frac{1}{2}}k^{-1}\sin\,(\tfrac{1}{2}\mathbf{k}\cdot\Delta\mathbf{r})\;\; Re\left\{A\,\exp\,i\left(\mathbf{k}\cdot\mathbf{r} - \omega t - \frac{\pi}{4}\right)\right\}kdkd\alpha.$$

For a continuous spectrum of waves, the mean square tension can be shown to equal

$$<F_{12}^2> \;= 4\rho\mu\iint \omega^3\,k^{-2}\sin^2\,(\tfrac{1}{2}\mathbf{k}\cdot\Delta\mathbf{r})\mathbf{S}kdkd\alpha.$$

For sufficiently large values of Δr, the $(\sin)^2$ factor, which oscillates rapidly, may be replaced by its average value, $\frac{1}{2}$, and the integration over α may be performed:

$$<F_\infty^2> \;= 2\rho\mu\int_0^\infty \omega^3\,k^{-2}\,\mathbf{T}_T dT.$$

Assuming the Neumann spectrum for $\mathbf{T}_T$, and setting $\omega^3k^{-2} = g^2T/2\pi$, (gravity waves) yields

$$<F_\infty^2> \;= \rho\mu\,\frac{(2\pi)^3cW^6}{32\,g^2} = 6\times 10^7\left(\frac{W}{10\text{ m sec}^{-1}}\right)^6(\text{dyne cm}^{-1})^2.$$

The required strength is therefore far in excess of 40 dynes/cm. But the large value reflects primarily the stresses due to the long period waves. To estimate the longest waves which will not readily rupture the film, we may set

$$2\rho\mu\int_0^{T_{\max}} \omega^3k^{-2}\mathbf{T}_T dT = (40\text{ dyne cm}^{-1})^2.$$

Neglecting capillary waves, this gives

$$T_{max} = (24)^{1/6}(2\pi)^{\frac{1}{3}}(\rho g^4 \mu c)^{-1/6}(40 \text{ dyne cm}^{-1})^{1/3} = 0.7 \text{ sec.}$$

The principal reduction in σ^2 by slicks has been attributed to waves of period greater than 0.7 sec (Fig. 7).

No allowance for generation and decay (other than by molecular processes) has been made in the present calculation. An alternate hypothesis for the effectiveness of slicks is that they damp only high frequency wave components and that, in absence of these components, the balance between generation and decay is thrown in favor of decay for low-frequency components. This matter needs further investigation.

7. THE SPECTRUM OF ACCELERATION

The horizontal acceleration of an elementary wave train, $A \cos (kx - \omega t)$, has an amplitude $\omega^2 A$ at the sea surface. For gravity waves this equals gkA. The slope has an amplitude kA. Except for a minor contribution from capillaries (see end of Section 5.4), *the distribution of acceleration (in units of g) and of slope (in radians) are equivalent:*[10]

$$a_c^2 = \sigma_c^2, \qquad a_u^2 = \sigma_u^2,$$

where a_c^2 and a_u^2 are the crosswind and up/downwind components of the mean square acceleration (in units of g) at the sea surface. The mean square horizontal acceleration, regardless of direction, is therefore

$$a_h^2 = a_c^2 + a_u^2 = \sigma^2.$$

The mean square vertical acceleration a_v^2 for deep water waves equals the horizontal acceleration, and the mean square acceleration in all three directions is

$$a^2 = a_h^2 + a_v^2 = 2\sigma^2.$$

Preceding results regarding the slope distribution can be applied directly. Thus the up/downwind component exceeds the crosswind component of mean square acceleration by a factor of 1.3, on the average; all mean square accelerations increase linearly with wind, and the total rms acceleration at a wind speed of 14 m sec^{-1} is 0.4 g!

The horizontal acceleration spectrum is $\omega^4 \mathrm{T}_T$, and the mean square acceleration,

$$a_h^2 = \int_0^\infty \omega^4 \mathrm{T}_T dT = \pi^3 \sqrt{\left(\frac{\pi}{2}\right)} \frac{cW}{2g},$$

varies *exactly* in proportion to wind speed according to the Neumann spectrum.

[10] This was first pointed out to us by N. F. Barber (personal communication).

REFERENCES

Arthur, R. S.

1949. Variability in the direction of wave travel. Ann. N. Y. Acad. Sci., *51:* 511–522.

Chandrasekhar, S.

1943. Stochastic problems in physics and astronomy. Rev. mod. Phys., *15:* 1–89.

Cox, Charles and W. H. Munk

1953. Air Force Technical Reports No. 2, 3, 4, SIO Ref. 52–61, 53–53, 54–10 (unpub).

1954. The measurement of the roughness of the sea surface from photographs of the sun's glitter. J. opt. Soc. Amer. (In press)

Darbyshire, J.

1952. The generation of waves by wind. Proc. Roy. Soc. (A) *215:* 299–328.

Duntley, S. Q.

1950. The visibility of submerged objects: Part I. Optical effects of water waves. Rep. Visibility Lab., Mass. Inst. Techn., Dec. 15, 1950; U. S. Off. Naval Res. Rep. No. N5 ori-07831.

Eckart, Carl

1953. The scattering of sound from the sea surface. J. acoust. Soc. Amer., *25:* 566–570.

Hennicker, J. C.

1949. The depth of the surface zone of a liquid. Rev. mod. Phys., *21:* 322–341.

Lamb, H.

1932. Hydrodynamics. Cambridge University Press, London. 738 pp.

Longuet-Higgins, M. S.

1950. A theory of the origin of microseisms. Phil. Trans., *243:* 1–35.

Neumann, G.

1953. On ocean wave spectra and a new method of forecasting wind generated sea. Technical Memoirs, Beach Erosion Board.

Pierson, W. J. and W. Marks

1952. The power spectrum analysis of ocean wave records. Trans. Amer. geophys. Un., *33:* 834–844.

Rice, S. O.

1944. Mathematical analysis of random noise. Bell Syst. tech. J., *23:* 282–332.

Schooley, A. H.

1954. A simple optical method for measuring the statistical distribution of water surface slopes. J. opt. Soc. Amer., *44:* 37–40.

Syōno, S.

1953. Frequency distribution functions of velocities in turbulent flow. J. met. Soc. Japan, *31:* 299–305.

Titchmarsh, E. C.

1937. Introduction to the theory of Fourier integrals. Oxford Clarendon Press, London. 390 pp.

Wiener, N.

1933. The Fourier integral and certain of its applications. Cambridge University Press, London. 201 pp.

THE USE OF ELECTRICAL CONDUCTIVITY MEASUREMENTS FOR CHLORINITY DETERMINATION[1]

By

M. J. POLLAK

Chesapeake Bay Institute, The Johns Hopkins University

ABSTRACT

Limitations in our knowledge of the electrical conductivity of sea water are discussed. An empirical equation is presented which gives chlorinity as a function of specific conductance and temperature at atmospheric pressure.

Determination of chlorinity of sea water by chemical analysis, while unsurpassed in accuracy, has always been a cumbersome technique and one which generally involves a considerable time lag between sampling and availability of results. An alternative method of determining chlorinity, or salinity, is the measurement of electrical conductivity (specific conductance) as a parameter of chlorinity and of the simultaneously measured temperature. Proof of the basic soundness of this method is furnished by the extended use of the shipboard electrical salinity bridge described by Wenner *et al.* (1930). Its accuracy is considered comparable to that of the Knudsen method of chlorinity titration ($\pm$ 0.02 ‰ of salinity). Since this instrument was designed for empirical calibration against samples of known salinity, the establishment of an exact relationship between specific conductance, chlorinity, and temperature was not required.

Increasing emphasis on *in situ* measurements that result in large quantities of data as well as the desirability of a sound basis of comparison between different sets of specific conductance measurements lend importance to the need for a unique functional relationship between the variables involved. It is the purpose of this note to draw attention to certain limitations in our present knowledge of this relationship and to present an empirical approximation to it which may facilitate the use of this type of data.

The basis for the conversion of most present-day oceanographic measurements of electrical conductivity is a table derived by Thomas *et al.* (1934) from their own experimental work which gives specific

[1] Contribution No. 19 from the Chesapeake Bay Institute. This work was supported by the Office of Naval Research (Geophysics Branch), the State of Maryland (Department of Research and Education), and the Commonwealth of Virginia (Virginia Fisheries Laboratory).

conductance as a function of chlorinity and temperature. From these data Jacobson (1948) developed an analytical function which, because of the approximations involved, is unsuited for accurate work. The only other major investigation of the electrical conductivity of sea water was carried out by Bein *et al.* (1935). Since the objective of Bein *et al.* was a comparison of direct density measurements with values computed from various parameters, their data are presented in a form not readily adaptable to the problem at hand.

The results obtained by Thomas *et al.* appear to contain errors from two sources. One of these, mentioned by the authors in a footnote, is the use of the Parker and Parker (1924) values for the specific conductance of a 0.1 demal potassium chloride solution (the reference standard for their conductivity measurements). Jones and Bradshaw (1933) had found that these Parker and Parker values were low by 0.118% at 0°C, by 0.028% at 18°C, and by 0.028% at 25°C. It can be presumed that the resulting errors in the Thomas *et al.* measurements are of the same magnitude.

The second source of errors is their use of Washburn pipet type conductivity cells. Jones and Bollinger (1931) found that in cells of this general design (Leeds and Northrup Co., 1924) there exists a capacitative shunt between parts of the cells of opposite polarity which results in resistance measurements that are lower than the true values. This so-called Parker Effect varies with the frequency, with the geometry of the cell, and with the resistance of the solution, but it always gives positive errors in conductivity. Although these errors in the Thomas *et al.* data are of unknown magnitude, it is apparent that they are of opposite sign from those due to the reference standards used. Thus the total error in those data might be either positive or negative.

Wenner *et al.* suggest that electrical conductivity may be a more accurate parameter of total salt content than of chlorinity alone. If this is the case, then the Thomas *et al.* data may reflect certain slight geographical differences not only in the conductivity-chlorinity relationship but in the chlorinity-salinity relationship established by Knudsen (1901). Minor anomalies of this nature are indicated, though not conclusively, by the works of Bein *et al.* and of Thompson and Wirth (1931). Jones and Bradshaw pointed out that absorbed carbon dioxide will increase the conductivity of a solution. Since dissolved CO_2 varies over a considerable range in the sea, this effect may be a source of additional small errors in field measurements of specific conductance.

Apparently the effect of pressure on the electrical conductivity of sea water has not been investigated, but it is a factor which cannot be

ignored when dealing with *in situ* measurements at depths of several hundred meters. From analogy with other physical properties of sea water it appears likely that this effect would become significant at a depth which will depend on the degree of accuracy of the measurements.

Despite the various gaps and uncertainties in our knowledge of the electrical conductivity of sea water, it was felt that the development of an analytical function relating specific conductance to chlorinity and temperature at atmospheric pressure would serve a useful purpose. The true physical relationship between these variables should be of the form $C = f(T, H)_{p=0}$, where C = specific conductance in mhos per cm^3 (the dimensions used by Thomas *et al.;* Jones and collaborators use the more conventional mhos per cm), T = temperature in°C, and H = chlorinity in ‰ (halide concentration determined by titration).

From a practical standpoint it is preferable to have a function giving H in terms of C and T. Such an empirical function was derived from the basic experimental data of Thomas *et al.*, and it is believed that it eliminates some slight discrepancies in their results which may well have been due to the above mentioned geographical anomalies.

The simplest form of this relationship is

$$H = \frac{K_1(T)}{C^{-1.07} - K_2(T)},$$

where $K_1(T) = \dfrac{6 \times 10^8}{721{,}392 + 24{,}597.1T - 29.17T^2 + 20.12T^3 - 0.974T^4 + 0.01584T^5}$

and $K_2(T) = K_1(T) \times \dfrac{5541 + 254.95T + 7.145T^2 - 0.73T^3 + 0.142T^4}{3{,}904{,}644}$.

While these two parametric functions of temperature gave the best fit of the data, their complexity may be due partly to the use of the Parker and Parker reference standards whose errors seem to vary rather unsystematically with temperature. In comparing chlorinities computed by means of this equation with the 61 titration values of the original data, the following results were obtained: in 32 cases the difference was 0.002 ‰ or less; in 22 cases it was between 0.003 and 0.005 ‰; and in the remaining 7 cases it varied from 0.007 to 0.027 ‰.

Because of the separation of variables, the above form of the equation lends itself to compact, yet comprehensive, tabulation—one table for each of the three terms. By means of various manipulations it can

be put into other forms which might be more suitable for restricted ranges of the variables or for lower requirements in accuracy.

It is a pleasure to acknowledge many fruitful discussions of the problem with D. E. Carritt and J. H. Carpenter of the Chesapeake Bay Institute.

REFERENCES

Bein, Willy, H.-G. Hirsekorn, Lotte Möller
1935. Konstantenbestimmungen des Meerwassers und Ergebnisse über Wasserkörper. Veröff. Inst. Meeresk., Univ. Berl. N. F., A. Geogr.-naturwiss. Reihe, *28*. 240 pp.

Jacobson, A. W.
1948. An instrument for recording continuously the salinity, temperature, and depth of sea water. Trans. Amer. Inst. elect. Engrs., *67:* 714.

Jones, Grinnell and G. M. Bollinger
1931. The measurement of the conductance of electrolytes. III. The design of cells. J. Amer. chem. Soc., *53:* 411.

Jones, Grinnell and B. C. Bradshaw
1933. The measurement of the conductance of electrolytes. V. A redetermination of the conductance of standard potassium chloride solutions in absolute units. J. Amer. chem. Soc., *55:* 1780.

Knudsen, Martin
1901. Hydrographical Tables. G. E. C. Gad, Copenhagen. 63 pp.

Leeds & Northrup Company
1924. Apparatus for measuring conductivity of electrolytes. Catalog No. 48, Philadelphia. 32 pp.

Parker, H. C. and E. W. Parker
1924. The calibration of cells for conductance measurements. III. Absolute measurements on the specific conductance of certain potassium chloride solutions. J. Amer. chem. Soc., *46:* 312.

Thomas, B. D. with T. G. Thompson and C. L. Utterback
1934. The electrical conductivity of sea water. J. Cons. int. Explor. Mer, *9:* 28.

Thompson, T. G. and H. E. Wirth
1931. The specific gravity of sea water at zero degrees in relation to the chlorinity. J. Cons. int. Explor. Mer, *6:* 232.

Wenner, Frank, E. H. Smith, and F. M. Soule
1930. Apparatus for the determination aboard ship of the salinity of sea water by the electrical conductivity method. J. Res. U. S. Bur. Standards, Paper No. 223, *5:* 711.